U.S. Department of Commerce
National Technical Information Service

N74 13715

AUTOMATIC CONTROL OF A HELICOPTER WITH A HANGING LOAD

NASA AMES RESEARCH CENTER
MOFFETT FIELD, CA

JUN 73

SUDAAR NO. 459

STANFORD UNIVERSITY

CENTER FOR SYSTEMS RESEARCH

Automatic Control of a Helicopter with a Hanging Load

by
Narendra K. Gupta
and
Arthur E. Bryson, Jr.

Guidance and Control Laboratory

June 1973

Prepared under
NAS 2-5143 for the U. S. Army
Air Research and Mobility Command
Ames Directorate
NASA Ames Research Center
Moffett Field, California

DEPARTMENT OF AERONAUTICS AND ASTRONAUTICS

AUTOMATIC CONTROL OF A HELICOPTER WITH A HANGING LOAD

by

Narendra K. Gupta

and

Arthur E. Bryson, Jr.

SUDAAR No. 459

June 1973

Department of Aeronautics and Astronautics
Stanford University
Stanford, California

Prepared under

NAS 2-5143 for the U. S. Army
Air Research and Mobility Command
Ames Directorate
NASA-Ames Research Center
Moffett Field, California

ABSTRACT

Helicopters are occasionally used to carry loads hanging below them on cables. Piloting the helicopter under these conditions is difficult, particularly when the mass of the load is comparable to that of the helicopter, and there are gusty winds. An autopilot logic is designed here for controlling a helicopter with a hanging load. A 16th order model for the system is decoupled into four subsystems: (a) A second order system for yawing motion, (b) a second order system for vertical motion, (c) a sixth order system for longitudinal motion, and (d) a sixth order system for lateral motion. A novel measuring scheme, which could be used in remote areas, is developed and filters are designed to estimate the state variables from these measurements.

The autopilot can be used to move the load over short distances without retracting the cables. This is done by automatically shifting the autopilot modes from position-hold (hover) to acceleration-hold to velocity-hold (cruise) to deceleration-hold to velocity-hold (near hover) to position-hold (hover). Use of such an autopilot might save considerable turnaround time.

The Sikorsky S-61 helicopter is chosen as an example vehicle. The performance of the controlled system is studied in the presence of longitudinal and lateral winds. Satisfactory response is obtained under design conditions and also with nominal changes in system parameters.

CONTENTS

LIST OF ILLUSTRATIONS

LIST OF TABLES

Chapter I

INTRODUCTION

A helicopter is an ideal vehicle for transporting heavy, bulky loads over short distances where surface transport is either infeasible or uneconomical, e.g., in off-loading containers from ships or carrying transmission towers or prefabricated buildings to remote sites. In many cases the load is so big that it cannot be carried inside the aircraft. Therefore it must be transported hanging from cables fastened to the aircraft. It might be carried in a hanging position to save loading and unloading time.

The pendulum modes of the hanging load couple into the motions of the helicopter to form an unstable system. The instability is not severe and an experienced pilot can still control the helicopter. However, the pilot work load is so great that it is almost impossible to add further tasks such as position-hold (precision hover), even in still air. On the other hand, an automatic control system can stabilize the system and perform additional tasks such as precision-hover even in gusty winds.

To simplify the autopilot design and implementation the complete motion is approximated by four uncoupled motions. A technique is developed for finding filter and controller gains. The Sikorsky S-61 is taken as the example helicopter.

For this system some changes in parameters are expected during a mission. Also some parameters may not be known accurately in advance. The effect of the parameters on system behavior is studied using a fixed set of filter and controller gains.

Chapter II develops the equations of motion for the system and describes the measuring technique near hover. The system definition matrices for the linearized system are given under design conditions.

Chapter III describes the design technique for controller and filter for the precision hover autopilot. The performance is studied

under design conditions.

Chapter IV suggests a technique for moving the hanging load over short distances. The load transfer is carried out in four steps involving speeding up, holding the speed, slowing down and precision hover.

Chapter V makes a study of the effects of changes in system parameters. Chapter VI summarizes the problem and the solution.

Chapter II

EQUATIONS OF MOTION

2.1 Introduction

A helicopter carrying a hanging load can be modeled as a system of three connected bodies: (a) Rotor, (b) Fuselage, and (c) Hanging load. The rotor can be tilted much faster than the fuselage or the cable carrying the hanging load. Since we are not interested in high frequency effects associated with rotor states, it suffices to use a quasi-steady rotor model. In this description it is assumed that the inclination of the rotor no-feathering plane (NFP) to the fuselage can be changed "instantaneously" using the cyclic pitch control. The hanging load is modeled as a point mass. Thus the dynamical system is simplified to one rigid body and a point mass (the vehicle and the hanging load).*

This mathematical model is of 16th order with four control variables. The state variables are: Three position and three translational velocity coordinates of the vehicle center of mass; three angular orientation and three angular velocity coordinates of the fuselage; two angular orientation and two angular velocity coordinates of the cable. The control variables are the longitudinal and lateral inclinations of the rotor NFP, the collective pitch, and the tail rotor. However, near hover, the yaw motion and the vertical motion are very nearly uncoupled from the longitudinal and the lateral motions. This results in a second order model for yaw motion with tail rotor as control, a second order model for vertical motion with collective pitch as control, and a 12th order model for longitudinal and lateral motions with longitudinal and lateral cyclic pitch as controls. We will later discuss the decoupling of the longitudinal motions from the lateral motions.

---

*In case the size of the hanging load is comparable to the length of the cable, the hanging load and the cable could be considered as a compound pendulum. The analysis is very similar and the number of state variables is the same.

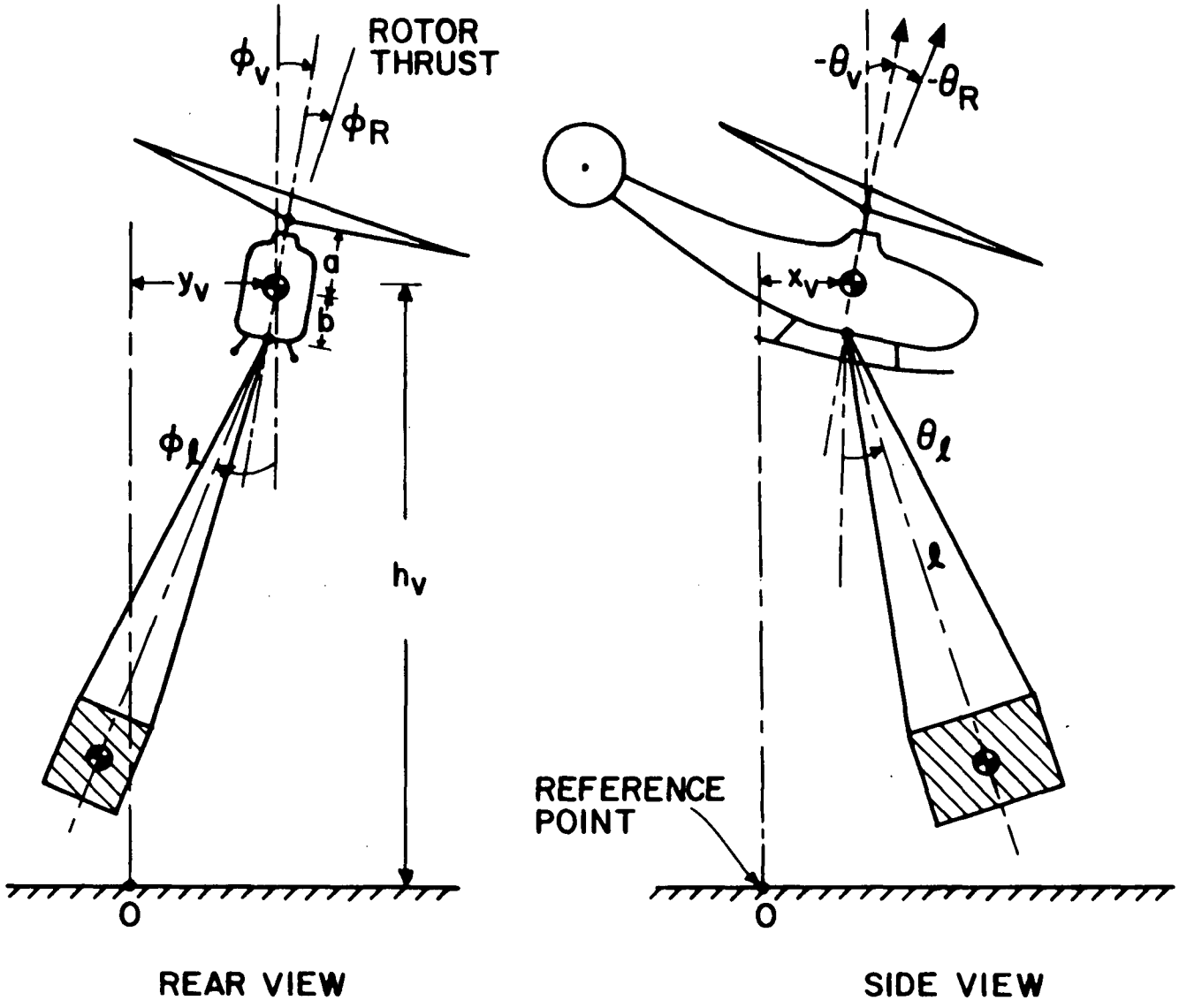

FIG. 2.1 Helicopter Carrying a Hanging Load

2.2 Equations of Motion

Figure 2.1 shows the coordinate system used to describe the motions of a helicopter carrying a hanging load. It is assumed that the load is carried by several cables attached to the helicopter at a point below its center of mass. Some important distances are shown in the figure.

Let

x,y,h = longitudinal, lateral, and vertical deviations from a desired point

u,v,w = three components of linear velocity

ϕ,θ,ψ = roll, pitch, and yaw angles

p,q,r = roll, pitch, and yaw rates

R,v,ℓ = subscripts for rotor, vehicle, and hanging load (or cable) respectively

$V_{w_x}, V_{w_y}, V_{w_z}$ = three components of wind velocity

$d_{(\cdot)}$ = aerodynamic damping coefficients

The kinetic energy of the system is

$$T = \frac{1}{2} m_v[\dot{x}_v^2+\dot{y}_v^2+\dot{h}_v^2] + \frac{1}{2} m_\ell[\dot{x}_\ell^2+\dot{y}_\ell^2+\dot{h}_\ell^2] + \frac{1}{2}[I_x\dot{\phi}_v^2+I_y\dot{\theta}_v^2+I_z\dot{\psi}_v^2] \tag{2.1}$$

and the potential energy is

$$V = m_v g h_v + m_\ell g h_\ell \tag{2.2}$$

The vertical position of the hanging load can be expressed in terms of other variables, thus

$$\begin{aligned} h_\ell &= h_v - b\cos\theta_v\cos\phi_v - \ell\cos\theta_\ell\cos\phi_\ell \\ &\approx h_v - b - \ell + \frac{b}{2}[\theta_v^2+\phi_v^2] + \frac{\ell}{2}[\theta_\ell^2+\phi_\ell^2] \end{aligned} \tag{2.3}$$

for small angles.

Also,

$$x_\ell = x_v + b\sin\theta_v + \ell\sin\theta_\ell \approx x_v + b\theta_v + \ell\theta_\ell$$

$$y_\ell \approx y_v - b\phi_v - \ell\phi_\ell$$

giving

$$\theta_\ell = (x_\ell - x_v - b\theta_v)/\ell \tag{2.4}$$

$$\phi_\ell = (-y_\ell + y_v - b\phi_v)/\ell \tag{2.5}$$

Thus the potential energy is

$$V = (m_v+m_\ell)gh_v - m_\ell g(b+\ell) + \frac{m_\ell g}{2}\left[b(\theta_v^2+\phi_v^2) + \ell\left\{\left(\frac{x_\ell - x_v - b\theta_v}{\ell}\right)^2 + \left(\frac{-y_\ell + y_v - b\phi_v}{\ell}\right)^2\right\}\right] \tag{2.6}$$

The independent coordinates are h_v ; ψ_v ; θ_v , x_v , x_ℓ and ϕ_v , y_v , y_ℓ . Using the generalized Lagrange method, the equations of motion can be written. The equation governing h_v is:

$$m_v\ddot{h}_v + m_\ell\ddot{h}_v + (m_v+m_\ell)g = T - m_v d_h(\dot{h}_v - V_{w_z})$$

Since the nominal value of vertical acceleration is zero

$$T_n \cong (m_v+m_\ell)g \tag{2.7}$$

where subscript n denotes nominal value.

If

$$T = T_n + \delta T \tag{2.8}$$

and

$$\gamma = \frac{m_v+m_\ell}{m_v} \tag{2.9}$$

we have

$$\boxed{\ddot{h}_v = \frac{\delta T}{\gamma m_v} - d_h\frac{(\dot{h}_v - V_{w_z})}{\gamma}} \tag{2.10}$$

The equation governing ψ_v is:

$$I_z\ddot{\psi}_v = \tau_t - \tau_m - I_z d_\psi\dot{\psi}_v \tag{2.11}$$

where τ_t is the torque produced by the tail rotor at the center of mass and τ_m is the torque of the main rotor

$$\boxed{\ddot{\psi}_v = \frac{\delta\tau_t}{I_z} - d_\psi \dot{\psi}_v} \tag{2.12}$$

The equations governing θ_v, x_v, and x_ℓ (longitudinal motions) are:

$$I_y\ddot{\theta}_v + m_\ell g b\theta_v + \frac{m_\ell g}{\ell}(x_\ell - x_v - b\theta_v)(-b)$$
$$= Ta\theta_R - \alpha_1 I_y\dot{\theta}_v + \sigma_1 I_y(\dot{x}_v - V_{w_x}) + \alpha_3 I_y\dot{\phi}_v + \sigma_3 I_y(\dot{y}_v - V_{w_y})$$
$$+ D_1\theta_R + D_2\phi_R \tag{2.13}$$

$$m_v\ddot{x}_v + \frac{m_\ell g}{\ell}(x_\ell - x_v - b\theta_v)(-1) = -T(\theta_v + \theta_R) + \alpha_2 m_v\dot{\theta}_v - \sigma_2 m_v(\dot{x}_v - V_{w_x})$$
$$- \alpha_4 m_v\dot{\phi}_v - \sigma_4 m_v(\dot{y}_v - V_{w_y}) - D_3\theta_R - D_4\phi_R \tag{2.14}$$

$$m_\ell\ddot{x}_\ell + \frac{m_\ell g}{\ell}[x_\ell - x_v - b\theta_v] = -m_\ell\sigma_5(\dot{x}_\ell - V_{w_x}) \tag{2.15}$$

The first term in the generalized force expressions on the right-hand side of equations (2.13) and (2.14) is due to rotor thrust, the next four terms represent damping and the last two terms arise from blade coning, offset distance of flapping hinge, and other effects. Expressions for D_1, D_2, D_3, and D_4 have been derived by Hall (H1). The only term on the right-hand side of equation (2.15) is due to air drag on the hanging load.

For small changes we can approximate T by T_n in the equations above. Thus, using (2.7) and (2.9), we have:

$$\ddot{\theta}_v + \frac{(\gamma-1)m_v gb}{I_y}\left[\frac{(b+\ell)}{\ell}\theta_v + \frac{x_v}{\ell} - \frac{x_\ell}{\ell}\right]$$

$$= \frac{\gamma m_v ga + D_1}{I_y}\theta_R + \frac{D_2}{I_y}\phi_R - \alpha_1\dot{\theta}_v + \sigma_1(\dot{x}_v - V_{w_x}) + \alpha_3\dot{\phi}_v + \sigma_3(\dot{y}_v - V_{w_y})$$

$$\ddot{x}_v + \left\{(\gamma-1)\frac{b}{\ell} + \gamma\right\} g\theta_v + \frac{(\gamma-1)g}{\ell}x_v - \frac{(\gamma-1)g}{\ell}x_\ell$$

$$= \left(-\gamma g - \frac{D_3}{m_v}\right)\theta_R - \frac{D_4}{m_v}\phi_R + \alpha_2\dot{\theta}_v - \sigma_2(\dot{x}_v - V_{w_x}) - \alpha_4\dot{\phi}_v - \sigma_4(\dot{y}_v - V_{w_y})$$

$$\ddot{x}_\ell - \frac{b}{\ell}g\theta_v - \frac{g}{\ell}x_v + \frac{g}{\ell}x_\ell = -(\gamma-1)\sigma_5(\dot{x}_\ell - V_{w_x})$$

(2.16)

The equations for ϕ_v, y_v, and y_ℓ (lateral motion) can be written in a similar manner:

$$\ddot{\phi}_v + \frac{(\gamma-1)m_v gb}{I_x}\left[\frac{(b+\ell)}{\ell}\phi_v - \frac{y_v}{\ell} + \frac{y_\ell}{\ell}\right] = \frac{\gamma m_v ga + D_1}{I_x}\phi_R - \frac{D_2}{I_x}\theta_R$$

$$- \alpha_1'\phi_v - \sigma_1'(\dot{y}_v - V_{w_y}) - \alpha_3'\dot{\theta}_v + \sigma_3'(\dot{x}_v - V_{w_x})$$

$$\ddot{y}_v - \left\{(\gamma-1)\frac{b}{\ell} + \gamma\right\} g\phi_v + \frac{(\gamma-1)g}{\ell}y_v - \frac{(\gamma-1)g}{\ell}y_\ell = \left(\gamma g + \frac{D_3}{m_v}\right)\phi_R - \frac{D_4}{m_v}\theta_R$$

$$- \alpha_2\dot{\phi}_v - \sigma_2(\dot{y}_v - V_{w_y}) - \alpha_4\dot{\theta}_v + \sigma_4(\dot{x}_v - V_{w_x})$$

$$\ddot{y}_\ell + \frac{b}{\ell}g\phi_v - \frac{g}{\ell}y_v + \frac{g}{\ell}y_\ell = -(\gamma-1)\sigma_5(\dot{y}_\ell - V_{w_y})$$

(2.17)

2.3 Decoupling into Subsystems

The complete system can be divided into three subsystems. They are:

(a) Yawing Motion: This is a second order system in which ψ_v and $\dot{\psi}_v$ are state variables and $\delta\tau_t$ is the control variable.

$$\frac{d}{dt}\begin{bmatrix}\psi_v\\ \dot{\psi}_v\end{bmatrix} = \begin{bmatrix}0 & 1\\ 0 & -d_\psi\end{bmatrix}\begin{bmatrix}\psi_v\\ \dot{\psi}_v\end{bmatrix} + \begin{bmatrix}0\\ 1/I_z\end{bmatrix}\delta\tau_t \qquad (2.18)$$

(b) Vertical Motion: This is a second order system with h_v and $\dot{h}_v$ as state variables and δT, related to the collective pitch, as the control variable.

$$\frac{d}{dt}\begin{bmatrix}h_v\\ \dot{h}_v\end{bmatrix} = \begin{bmatrix}0 & 1\\ 0 & \frac{-d_h}{\gamma}\end{bmatrix}\begin{bmatrix}h_v\\ \dot{h}_v\end{bmatrix} + \begin{bmatrix}0\\ \frac{1}{\gamma m_v}\end{bmatrix}\delta T + \begin{bmatrix}0\\ \frac{d_h}{\gamma}\end{bmatrix}V_{w_z} \qquad (2.19)$$

(c) Longitudinal and Lateral Motions: These motions are described by a 12th order mathematical model with two controls. The state vector, $\underline{x}$, is

$$\underline{x}^T = (\theta_v, \dot{\theta}_v, x_v, \dot{x}_v, x_\ell, \dot{x}_\ell, \phi_v, \dot{\phi}_v, y_v, \dot{y}_v, y_\ell, \dot{y}_\ell) ,$$

the control vector $\underline{u} = (\theta_R, \phi_R)$ and the noise vector $\underline{w} = (V_{w_x}, V_{w_y})$. The state equation is

$$\dot{\underline{x}} = F\underline{x} + G\underline{u} + \Gamma\underline{w} \qquad (2.20)$$

Matrices $F(12\times12)$, $G(12\times2)$, and $\Gamma(12\times2)$ are given in Table II-1.

The models describing the vertical motion and yawing motion are simple second order systems. It is quite straightforward to design control laws for these systems. We will focus our attention on designing a control law for the system describing the lateral and longitudinal motions.

2.4 Decoupling the Longitudinal from the Lateral Motions

Referring to Table II-1, we see that the equations governing the longitudinal and lateral motions are coupled by cross-damping torques and forces. If we assume that θ_R primarily controls the longitudinal motions and ϕ_R primarily controls the lateral mations, there is an additional coupling in the closed loop system because ϕ_R produces a

Table II-1

System Definition Matrices

$\dot{\underline{x}} =$ **State Transition Matrix** $\underline{x} +$ **Control Distribution Matrix** $\underline{u} +$ **Wind Disturbance Distribution Matrix** $\underline{w}$

$\dot{\underline{x}}$	$\underline{x}^T$												$\underline{u}^T$		$\underline{w}^T$	
	θ_v	$\dot{\theta}_v$	x_v	$\dot{x}_v$	x_ℓ	$\dot{x}_\ell$	Φ_v	$\dot{\Phi}_v$	y_v	$\dot{y}_v$	y_ℓ	$\dot{y}_\ell$	θ_R	Φ_R	V_{w_x}	V_{w_y}
$\dot{\theta}_v$	0	1	0	0	0	0	0	0	0	0	0	0	0	0	0	0
$\ddot{\theta}_v$	$-\beta_1\frac{(b+\ell)}{\ell}$	$-\alpha_1$	$-\beta_{1/\ell}$	σ_1	$\frac{\beta_1}{\ell}$	0	0	α_3	0	σ_3	0	0	$\frac{\gamma m_v ga+D_1}{I_y}$	$+\frac{D_2}{I_y}$	$-\sigma_1$	$-\sigma_3$
$\dot{x}_v$	0	0	0	1	0	0	0	0	0	0	0	0	0	0	0	0
$\ddot{x}_v$	$-\beta_2$	α_2	$-\beta_3$	$-\sigma_2$	β_3	0	0	$-\alpha_4$	0	$-\sigma_4$	0	0	$-\gamma g-\frac{D_3}{m_v}$	$-\frac{D_4}{m_v}$	σ_2	σ_4
$\dot{x}_\ell$	0	0	0	0	0	1	0	0	0	0	0	0	0	0	0	0
$\ddot{x}_\ell$	$\frac{b}{\ell}g$	0	$\frac{g}{\ell}$	0	$\frac{-g}{\ell}$	$-(\gamma-1)\sigma_5$	0	0	0	0	0	0	0	0	$(\gamma-1)\sigma_5$	0
$\dot{\Phi}_v$	0	0	0	0	0	0	0	1	0	0	0	0	0	0	0	0
$\ddot{\Phi}_v$	0	$-\alpha_3'$	0	σ_3'	0	0	$-\beta_1'\frac{(b+\ell)}{\ell}$	$-\alpha_1'$	$\frac{\beta_1'}{\ell}$	$-\sigma_1'$	$-\frac{\beta_1'}{\ell}$	0	$-\frac{D_2}{I_x}$	$\frac{\gamma m_v ga+D_1}{I_x}$	$-\sigma_3'$	σ_1'
$\dot{y}_v$	0	0	0	0	0	0	0	0	0	1	0	0	0	0	0	0
$\ddot{y}_v$	0	$-\alpha_4$	0	σ_4	0	0	β_2	$-\alpha_2$	$-\beta_3$	$-\sigma_2$	β_3	0	$-\frac{D_4}{m_v}$	$\gamma g+\frac{D_3}{m_v}$	$-\sigma_4$	σ_2
$\dot{y}_\ell$	0	0	0	0	0	0	0	0	0	0	0	1	0	0	0	0
$\ddot{y}_\ell$	0	0	0	0	0	0	$\frac{-b}{\ell}g$		$\frac{g}{\ell}$	0	$\frac{-g}{\ell}$	$-(\gamma-1)\sigma_5$	0	0	0	$(\gamma-1)\sigma_5$

where

$$\beta_1 = \frac{(\gamma-1)m_v gb}{I_y}$$

$$\beta_2 = \left\{(\gamma-1)\frac{b}{\ell} + \gamma\right\} g$$

$$\beta_3 = \frac{(\gamma-1)g}{\ell}$$

$$\beta_1' = \frac{(\gamma-1)m_v gb}{I_x}$$

$$\gamma = \frac{m_\ell + m_v}{m_v}$$

small pitching moment and a small longitudinal force (in addition to producing large rolling moment and lateral force), while θ_R produces a small rolling moment and a small lateral force (in addition to producing large pitching moment and longitudinal force). However, a certain linear combination of θ_R and ϕ_R produces large pitching moment and longitudinal force, a small rolling moment and no lateral force. Another linear combination produces large rolling moment and lateral force, a small pitching moment and no longitudinal force. If we take these two linear combinations as control variables, the longitudinal-lateral decoupling approximation is quite good for the purpose of designing controllers and filters.

2.5 Measurements for Estimating the State Variables

All of the state variables in the system presented in the last section are observable from measurements of the position of the vehicle center of mass (or the sling load). However, with these measurements alone, the errors in the angular orientation estimates are large even if a relatively accurate position measurement is available. Hence, it is almost essential to also have measurements of vehicle and cable angles.

The position measurement technique suggested here consists of a second cable (a "measurement cable") fastened to a point on the ground, which passes through a ring mounted elastically in the plane of the aircraft floor, and is held by a constant tension winch inside the aircraft (Figure 2.2a). The portion of the cable above the aircraft floor is parallel to a reference axis fixed in the aircraft. The forces in the springs are measured using strain gauges, while a potentiometer in the constant tension winch measures the length of the cable. The nomenclature for the measurement cable is shown in Figure 2.2b. Let θ_m and ϕ_m be the inclinations of the rope to the aircraft reference axis and L_m, the length of the cable. Then neglecting the small deflections of the springs

$$x_m \hat{i} + \vec{L}_m - b_m \hat{k}_v = x_v \hat{i} + y_v \hat{j} - h_v \hat{k} \qquad (2.21)$$

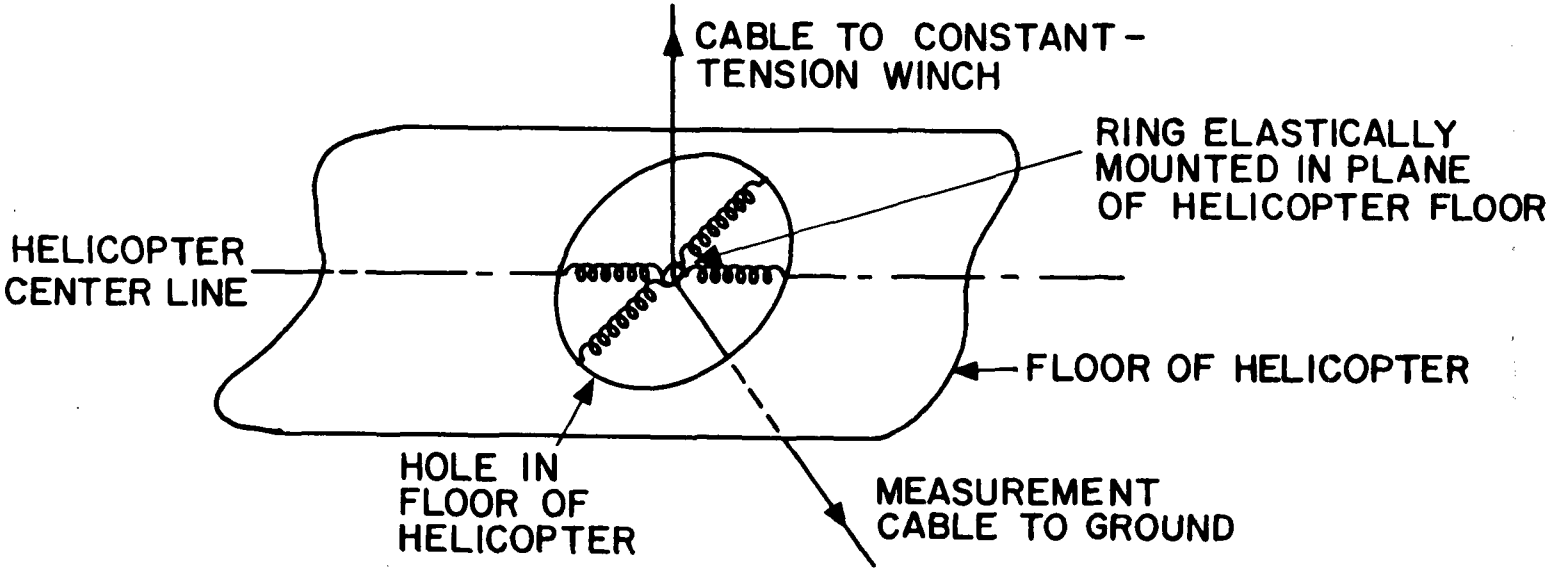

FIG. 2.2a Measurement Technique

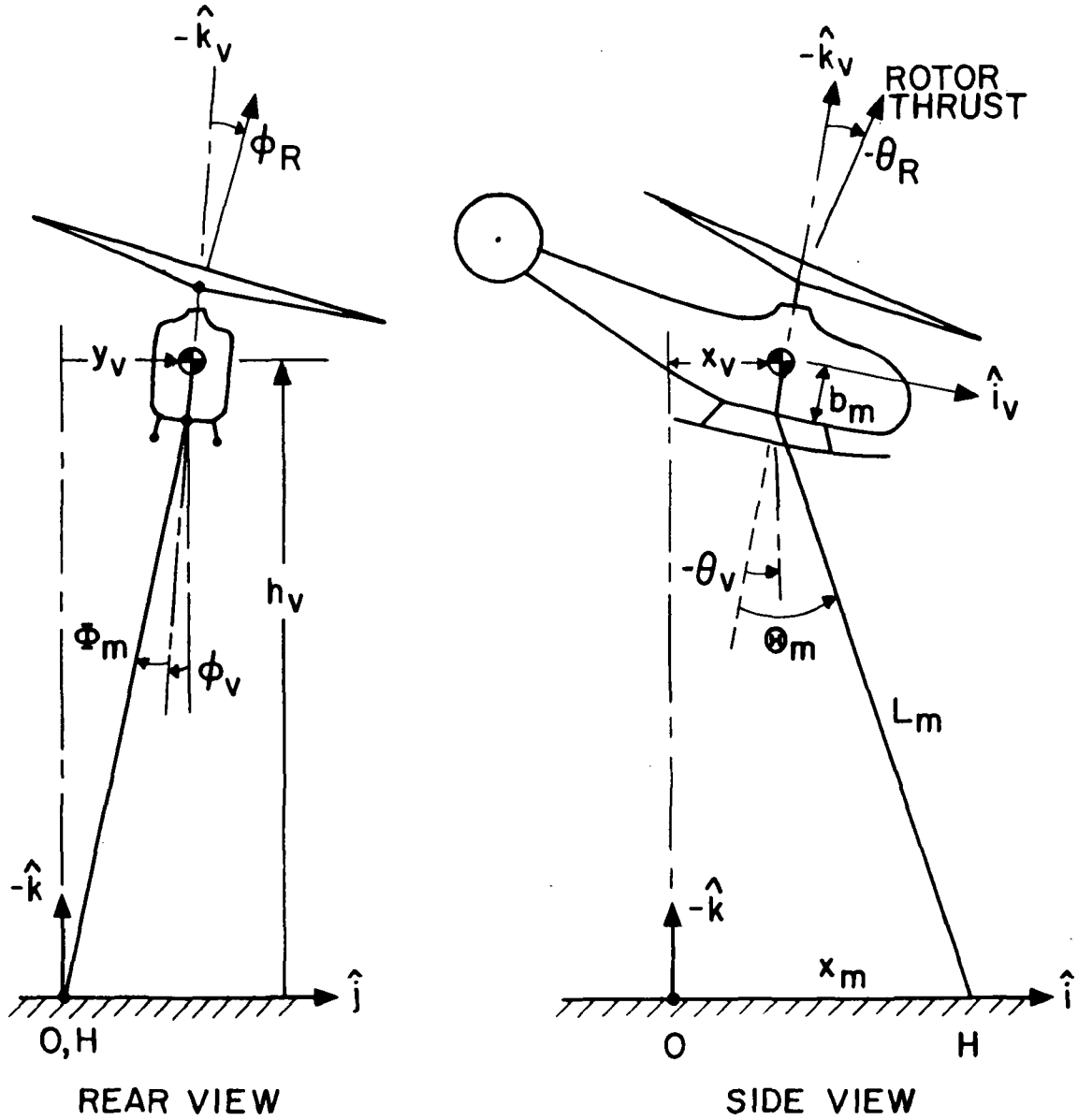

FIG. 2.2b Nomenclature for Measurement Cable

where

$$\vec{L}_m = \frac{L_m}{\sqrt{1+\tan^2\Theta_m+\tan^2\Phi_m}} \left[-\tan\Theta_m \ , \ \tan\Phi_m \ , \ -1\right] \begin{bmatrix} \hat{i}_v \\ \hat{j}_v \\ \hat{k}_v \end{bmatrix} \tag{2.22}$$

and the transformation between $\hat{i}$, $\hat{j}$, $\hat{k}$, and $\hat{i}_v$, $\hat{j}_v$, and $\hat{k}_v$ for small angular inclinations of the aircraft is

$$\begin{bmatrix} \hat{i}_v \\ \hat{j}_v \\ \hat{k}_v \end{bmatrix} = \begin{bmatrix} 1 & \psi_v & -\theta_v \\ -\psi_v & 1 & \phi_v \\ \theta_v & -\phi_v & 1 \end{bmatrix} \begin{bmatrix} \hat{i} \\ \hat{j} \\ \hat{k} \end{bmatrix} \tag{2.23}$$

Using this transformation in equation (2.22),

$$\vec{L}_m = \frac{L_m}{\sqrt{1+\tan^2\Theta_m+\tan^2\Phi_m}} \left[-\tan\Theta_m \ , \ \tan\Phi_m \ , \ -1\right] \begin{bmatrix} 1 & \psi_v & -\theta_v \\ -\psi_v & 1 & \phi_v \\ \theta_v & -\phi_v & 1 \end{bmatrix} \begin{bmatrix} \hat{i} \\ \hat{j} \\ \hat{k} \end{bmatrix} \tag{2.24}$$

Substituting (2.23) and (2.24) in (2.21) and equating components, we get

$$x_v = x_m - b_m\theta_v - \frac{L_m}{\sqrt{1+\tan^2\Theta_m+\tan^2\Phi_m}} (\tan\Theta_m+\theta_v-\psi_v\tan\Phi_m) \tag{2.25}$$

$$y_v = b_m\phi_v + \frac{L_m}{\sqrt{1+\tan^2\Theta_m+\tan^2\Phi_m}} (\tan\Phi_m+\phi_v-\psi_v\tan\Theta_m) \tag{2.26}$$

$$h_v = b_m + \frac{L_m}{\sqrt{1+\tan^2\Theta_m+\tan^2\Phi_m}} (1-\theta_v\tan\Theta_m-\phi_v\tan\Phi_m) \tag{2.27}$$

At nominal location and orientation

$$x_v=y_v=0 \ , \quad L_m=L_o \ , \quad \phi_v=\theta_v=\psi_v=0 \ ;$$

thus

$$\Phi_o=0 \ , \quad x_m=L_o\sin\Theta_o \ , \quad h_{v_o}=L_o\cos\Theta_o+b_m \tag{2.28}$$

Linearizing (2.25) - (2.27) about these nominal values gives

$$x_v \cong -(b_m+L_o\cos\Theta_o)\theta_v - L_o\cos\Theta_o\theta_m - \sin\Theta_o\ell_m \tag{2.29}$$

$$y_v \cong (b_m+L_o\cos\Theta_o)\phi_v + L_o\cos\Theta_o\phi_m - L_o\sin\Theta_o\psi_v \tag{2.30}$$

$$\delta h_v \cong \cos\Theta_o\ell_m - L_o\sin\Theta_o\theta_v \tag{2.31}$$

where

$$\ell_m=L_m-L_o\ , \quad \theta_m=\Theta_m-\Theta_o \quad \text{and} \quad \phi_m=\phi_m-0 \tag{2.32}$$

Solving (2.29) - (2.31) for θ_m , ϕ_m and ℓ_m we have,

$$\ell_m \cong \sec\Theta_o\delta h_v + L_o\tan\Theta_o\theta_v \tag{2.33}$$

$$\phi_m \cong \frac{\sec\Theta_o}{L_o}y_v - (1+\frac{b_m}{L_o}\sec\Theta_o)\phi_v + \tan\Theta_o\psi_v \tag{2.34}$$

$$\theta_m \cong -\sec\Theta_o(\sec\Theta_o+\frac{b_m}{L_o})\theta_v - \frac{\sec\Theta_o}{L_o}x_v + \tan\Theta_o\delta h_v \tag{2.35}$$

The angles between the cable carrying the hanging load and the fuselage reference axis could be measured in the same way using another elastically mounted ring. Thus

$$\begin{aligned}\theta_{\ell m} &= \theta_\ell-\theta_v = -\theta_v(1+\frac{b}{\ell}) - \frac{x_v}{\ell} + \frac{x_\ell}{\ell}\\ \phi_{\ell m} &= \phi_\ell-\phi_v = -\phi_v(1+\frac{b}{\ell}) + \frac{y_v}{\ell} - \frac{y_\ell}{\ell}\end{aligned} \tag{2.36}$$

The fuselage attitude could be obtained using an onboard vertical gyro. This gives measurements of θ_v and ϕ_v .

All these measurements contain errors. We model them as additive white noise. The measurement vector $\underline{z}$ for the two systems can be written as

$$\underline{z} = H\underline{x} + \underline{v}$$

where the matrix H for the longitudinal and lateral systems is given

in Table II-2*, $\underline{x}$ is the state vector, and

$$E[\underline{v}(t)\underline{v}^T(\tau)] = R\,\delta(t-\tau) \tag{2.37}$$

Table II-2

Measurement Distribution Matrix H

Longitudinal System

$$\begin{bmatrix} -\sec\Theta_o\left(\sec\Theta_o + \frac{b_m}{L_o}\right) & 0 & -\frac{\sec\Theta_o}{L_o} & 0 & 0 & 0 \\ -1-b/\ell & 0 & -1/\ell & 0 & 1/\ell & 0 \\ 1 & 0 & 0 & 0 & 0 & 0 \end{bmatrix}$$

Lateral System

$$\begin{bmatrix} -1-\frac{b_m}{L_o}\sec\Theta_o & 0 & \frac{\sec\Theta_o}{L_o} & 0 & 0 & 0 \\ -1-b/\ell & 0 & 1/\ell & 0 & -1/\ell & 0 \\ 1 & 0 & 0 & 0 & 0 & 0 \end{bmatrix}$$

The measurements and the power spectral densities of the additive white noises are summarized in Table II-3.

*It is assumed that ψ_v and h_v are determined accurately by separate measurements or another filter.

Table II-3

Measurements

MEASUREMENT	SYMBOL	LINEAR COMBINATION OF	SPECTRAL DENSITY OF ADDITIVE NOISE
1. Inclinations of Measurement Cable	θ_m	x_v , θ_v and δh_v	6×10^{-5} (rad)^{2}sec*
	ϕ_m	y_v , ϕ_v and ψ_v	6×10^{-5} (rad)^{2}sec
2. Inclinations of Load Cable	θ_{ℓ_m}	x_v , x_ℓ and θ_v	6×10^{-5} (rad)^{2}sec
	ϕ_{ℓ_m}	y_v , y_ℓ and ϕ_v	6×10^{-5} (rad)^{2}sec
3. Fuselage Attitude (from onboard gyros)	θ_v	θ_v	1.5×10^{-5}(rad)^{2}sec
	ϕ_v	ϕ_v	1.5×10^{-5}(rad)^{2}sec
4. Length of Measurement Cable	ℓ_m	δh_v and θ_v	.01 m^{2}sec**

* This corresponds to a noise with RMS 2 degree and correlation time .025 sec

** This corresponds to a noise with RMS .45m and correlation time .025 sec

2.6 System Definition Matrices for the Example Helicopter

To illustrate the technique of designing the control system, we have taken a 6000 kg Sikorsky S-61 as the example helicopter. It carries a 2000 kg hanging load on a 20 m long cable, attached to a point 1.5 m below its center of mass. The measurement cable is 35 m long and is offset 25 m in the longitudinal direction from the reference point on the ground. The state definition matrices F, G, and Γ are given in Table II-4 for the longitudinal-lateral motions of this system. Values of stability derivatives for this vehicle are taken from Hall and Bryson (H3). The drag coefficient on the hanging load is estimated assuming a reasonable size and drag coefficient and taking secant slope between zero and 7.0 m sec^{-1} wind velocity*.

The control vector is redefined so that its two components are linear combinations of θ_R and Φ_R as explained in section 2.4. If $\underline{u} = (\theta_R + .03\Phi_R\ ,\ \Phi_R - .03\theta_R)$ the control distribution matrix is modified from G_o to G as shown in Table II-4.

The decoupling approximation is made. The control u_1 affects the longitudinal motion and u_2 the lateral motion. The state definition matrices for the longitudinal and the lateral system are the appropriate portions of the matrices in Table II-4. Table II-5 gives H, the measurement distribution matrix.

Figure 2.3 shows the eigenvalues of the uncontrolled longitudinal and lateral systems. Also shown are the corresponding eigenvalues from the coupled 12th order system. The eigenvalue identification is done using the eigenvectors. The eigenvalues from the coupled and the decoupled system are very near to each other showing that the decoupling approximation is valid.

---

*The drag on a body depends on the square of the velocity. The slope of the drag vs. velocity curve at zero velocity is zero.

Table II-4

State Definition Matrices for One Version of Sikorsky S-61 Carrying a 2000 kg Hanging Load

$\dot{x}$	F												G_o		Γ		G	
θ_v	0.0	1.0	0.0	0.0	0.0	0.0	0.0	0.0	0.0	0.0	0.0	0.0	0.0	0.0	0.0	0.0	0.0	0.0
$\dot{\theta}_v$	-2.25	- .415	- .104	.0111	.104	0.0	0.0	.318	0.0	.00381	0.0	0.0	8.38	.393	- .0111	- .00381	8.38	.139
x_v	0.0	0.0	0.0	1.0	0.0	0.0	0.0	0.0	0.0	0.0	0.0	0.0	0.0	0.0	0.0	0.0	0.0	0.0
$\dot{x}_v$	-13.3	1.43	- .164	- .0198	.164	0.0	0.0	- .311	0.0	- .0059	0.0	0.0	-13.1	- .396	.0198	.0059	-13.1	0.0
x_ℓ	0.0	0.0	0.0	0.0	0.0	1.0	0.0	0.0	0.0	0.0	0.0	0.0	0.0	0.0	0.0	0.0	0.0	0.0
$\dot{x}_\ell$	.736	0.0	.491	0.0	- .491	- .0026	0.0	0.0	0.0	0.0	0.0	0.0	0.0	0.0	.0026	0.0	0.0	0.0
Φ_v	0.0	0.0	0.0	0.0	0.0	0.0	0.0	1.0	0.0	0.0	0.0	0.0	0.0	0.0	0.0	0.0	0.0	0.0
$\dot{\Phi}_v$	0.0	-1.23	0.0	.0136	0.0	0.0	- 8.28	-1.58	.385	- .0407	- .385	0.0	- 1.43	30.7	- .0136	.0407	- .465	30.8
y_v	0.0	0.0	0.0	0.0	0.0	0.0	0.0	0.0	0.0	1.0	0.0	0.0	0.0	0.0	0.0	0.0	0.0	0.0
$\dot{y}_v$	0.0	- .311	0.0	.0059	0.0	0.0	13.3	-1.43	- .164	- .0198	.164	0.0	- .396	13.1	- .0059	.0198	0.0	13.1
y_ℓ	0.0	0.0	0.0	0.0	0.0	0.0	0.0	0.0	0.0	0.0	0.0	1.0	0.0	0.0	0.0	0.0	0.0	0.0
$\dot{y}_\ell$	0.0	0.0	0.0	0.0	0.0	0.0	- .736	0.0	.491	0.0	- .491	- .0026	0.0	0.0	0.0	.0026	0.0	0.0
	$[\theta_v$	$\dot{\theta}_v$	x_v	$\dot{x}_v$	x_ℓ	$\dot{x}_\ell$	Φ_v	$\dot{\Phi}_v$	y_v	$\dot{y}_v$	y_ℓ	$\dot{y}_\ell]$	$[\theta_R$	$\Phi_R]$	$[v_{w_x}$	$v_{w_y}]$	$[\theta_R+.03\Phi_R, \Phi_R-.03\theta_R]$	
							$\underline{x}^T$						$\underline{u}_o^T$		$\underline{w}$		$\underline{u}^T$	

Units in meters, secs, radians

Table II-5

Measurement Definition Matrices for the Longitudinal System

$\underline{x}$ ↓	H^T:		
θ_v	-1.537	-1.075	1.0
$\dot{\theta}_v$	0.0	0.0	0.0
x_v	-.0348	-.05	0.0
$\dot{x}_v$	0.0	0.0	0.0
x_ℓ	0.0	+.05	0.0
$\dot{x}_\ell$	0.0	0.0	0.0
	$\underline{z} = [\theta_m$	θ_{ℓ_m}	$\theta_v]$

Measurement Definition Matrices for the Lateral System

$\underline{x}$ ↓	H^T:		
ϕ_v	-1.052	-1.075	1.0
$\dot{\phi}_v$	0.0	0.0	0.0
y_v	.0348	.05	0.0
$\dot{y}_v$	0.0	0.0	0.0
y_ℓ	0.0	-.05	0.0
$\dot{y}_\ell$	0.0	0.0	0.0
	$\underline{z} = [\phi_m$	ϕ_{ℓ_m}	$\phi_v]$

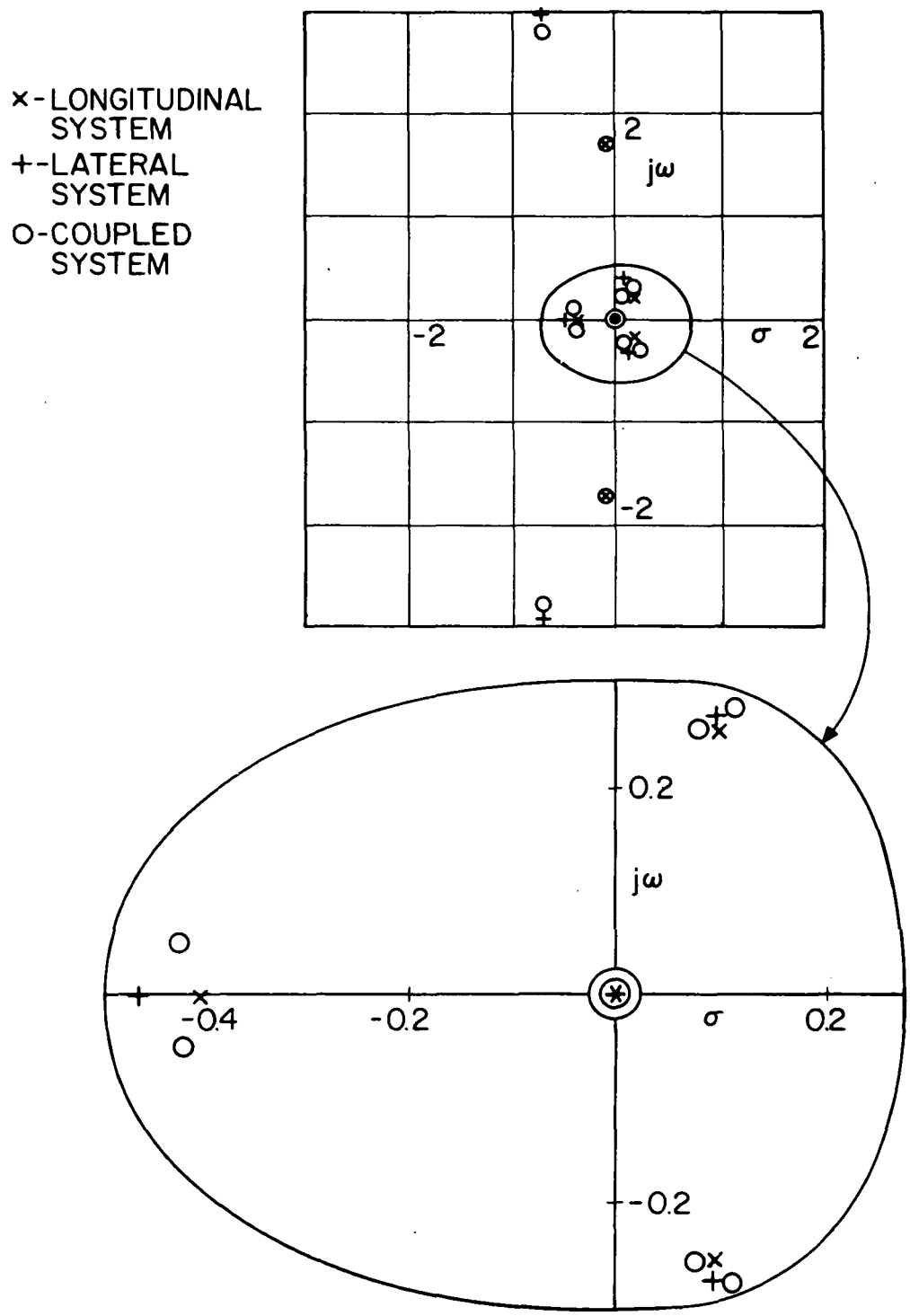

FIG. 2.3 Poles of the Open-Loop System

Chapter III

DESIGN AND PERFORMANCE OF A PRECISION HOVER AUTOPILOT

3.1 Introduction

The control logic for the longitudinal-lateral motions is designed using quadratic synthesis and neglecting the cross-coupling of these two motions. The wind velocities are modeled as exponentially correlated, i.e., as first order continuous Markov processes. To test the decoupling approximation, the control logic is used with the cross-coupled system model; the eigenvalues of this closed loop system are quite close to those predicted when neglecting the cross-coupling, though the eigenvectors are strongly coupled.

The performance of the system is first determined in the presence of winds assuming perfect state information (ideal case).

Next, optimal filters are designed for the longitudinal and lateral systems using the measurements shown in Table II-3. The root-mean-square (RMS) values of state and control variables are found using the filters combined with the control logic designed before. The transfer functions of the filter-controllers (compensators) are determined and are shown to be non-minimum phase.

If there is a steady wind disturbance the use of the control system above results in a steady state error. This steady state error can be avoided by using integral control, i.e., by adjoining a new state variable to the longitudinal system and another to the lateral system. For the longitudinal system the new state variable ξ is defined as

$$\dot{\xi} = x_{\ell} \tag{3.1}$$

This leads to zero error in the position of the hanging load in the presence of a steady wind.

3.2 Controller Design for Exponentially Correlated Wind

The correlation time of the wind velocity changes is usually comparable to or larger than the time constants associated with the controlled system. Therefore the wind disturbances cannot be modeled as "white noise". Hence, we model the head wind and crosswind as exponentially correlated with a 5 sec time constant, i.e.,

$$\dot{V}_{w_x} = -\frac{V_{w_x}}{\tau_c} + \eta_x \quad , \quad \tau_c = 5 \text{ sec}$$

Therefore,

$$\dot{V}_{w_x} = -.2V_{w_x} + \eta_x \tag{3.2}$$

η_x is white noise. If the RMS value of V_{w_x} is 7 m sec^{-1} the required spectral density of η_x is

$$R_{\eta_x} = \frac{2\times 7^2}{5} = 19.6 \text{ m}^2 \text{ sec}^{-3} \tag{3.3}$$

There is, of course, another equation like (3.2) for the crosswind disturbance.

If (3.2) is adjoined to the longitudinal dynamics equations the system is modified to

$$\frac{d}{dt}\begin{bmatrix} \underline{x} \\ \hdashline V_{w_x} \end{bmatrix} = \left[\begin{array}{c:c} F & \Gamma \\ \hdashline 0 & -1/\tau_c \end{array}\right]\begin{bmatrix} \underline{x} \\ \hdashline V_{w_x} \end{bmatrix} + \begin{bmatrix} G \\ \hdashline 0 \end{bmatrix} \underline{u} + \begin{bmatrix} 0 \\ \hdashline 1 \end{bmatrix} \eta_x \tag{3.4}$$

where $\underline{x}$, $\underline{u}$, F , Γ , and G are defined in Tables II-4 and II-5. We choose a control law such that $\underline{u}$ is a linear combination of $\underline{x}$ and V_{w_x} , i.e.,

$$\underline{u} = C\underline{x} + c_{w_x} V_{w_x} \tag{3.5}$$

$\underline{u}$ is a scalar in this case; hence, C is a row vector and c_{w_x} is a scalar. Substituting for $\underline{u}$ in (3.4) we have

$$\frac{d}{dt}\begin{bmatrix} \underline{x} \\ \hline V_{w_x} \end{bmatrix} = \left[\begin{array}{c|c} F+GC & \Gamma+Gc_{w_x} \\ \hline 0 & -1/\tau_c \end{array}\right]\begin{bmatrix} \underline{x} \\ \hline V_{w_x} \end{bmatrix} + \begin{bmatrix} 0 \\ \hline 1 \end{bmatrix}\eta_x \qquad (3.6)$$

Notice that the closed loop eigenvalues depend on state definition matrices and the gains C and do not depend on gain c_{w_x}. We can choose gains C and c_{w_x} independently; C to obtain the desired dynamics of the closed loop system, and c_{w_x} to achieve good performance in the presence of wind.

In the design procedure adopted here gains C are chosen using the quadratic synthesis procedure, i.e., by minimizing a performance index, J which is quadratic in state and control variables. The gain c_{w_x} can be chosen in several different ways. We have tried two of them here:

(1) Using the augmented state model with the desired performance index, quadratic synthesis gives the gain c_w in the same way as gains C. Quadratic synthesis strikes a compromise between the amount of control required and state variable deviations.

(2) In this procedure c_{w_x} is chosen to minimize the steady state RMS value of a desired linear combination of state variables (in this case the error in position of the hanging load). Thus, the control on wind can be tightened without making the closed-loop system too "fast". This procedure is described in detail in Appendix C.

The feedback gains on the state variables and wind velocity are shown in Table III-1 for both longitudinal and lateral systems. The gains on wind velocity are computed using both procedures.

The closed loop eigenvalues of the longitudinal and lateral systems are compared with the closed loop eigenvalues of the coupled longitudinal-lateral system (using gains from the decoupled systems) in Table III-1. The eigenvalues are quite close showing that the decoupling approximation is reasonable.

Table III-1

Controller for Exponentially Correlated Wind

$$J_{\text{longitudinal}} = E\left\{\left(\frac{\theta_v}{.2}\right)^2 + \left(\frac{x_v}{2}\right)^2 + \left(\frac{x_\ell}{1.0}\right)^2 + \left(\frac{u_1}{.1}\right)^2\right\}_{s.s.}$$

$$J_{\text{lateral}} = E\left\{\left(\frac{\phi_v}{.2}\right)^2 + \left(\frac{y_v}{2}\right)^2 + \left(\frac{y_\ell}{1.0}\right)^2 + \left(\frac{u_2}{.1}\right)^2\right\}_{s.s.}$$

Feedback Gains

c_{θ_v}	$c_{\dot{\theta}_v}$	c_{x_v}	$c_{\dot{x}_v}$	c_{x_ℓ}	$c_{\dot{x}_\ell}$	c_{ϕ_v}	$c_{\dot{\phi}_v}$	c_{y_v}	$c_{\dot{y}_v}$	c_{y_ℓ}	$c_{\dot{y}_\ell}$
-1.27	-.277	.141	.157	-.0296	.137	-.834	-.125	-.137	-.131	.0249	-.14

Feedback Gains on Wind

Technique	c_{w_x}	c_{w_y}
1	.00219	-.00208
2	.00239	-.00228

Closed Loop Eigenvalues of Coupled and Decoupled Systems

7th Order Longitudinal System [sec^{-1}]	7th Order Lateral System [sec^{-1}]	Complete 14th Order System [sec^{-1}]
-.99 ± 1.8j		-.93 ± 1.9j
-.58 ± 1.0j		-.57 ± 1.1j
-.84 ± .78j		-.91 ± .62j
	-2.2 ± 3.5j	-2.3 ± 3.5j
	-.82 ± .74j	-.72 ± .79j
	-.53 ± 1.0j	-.50 ± .98j
-.2	-.2	-.2*

* Double root

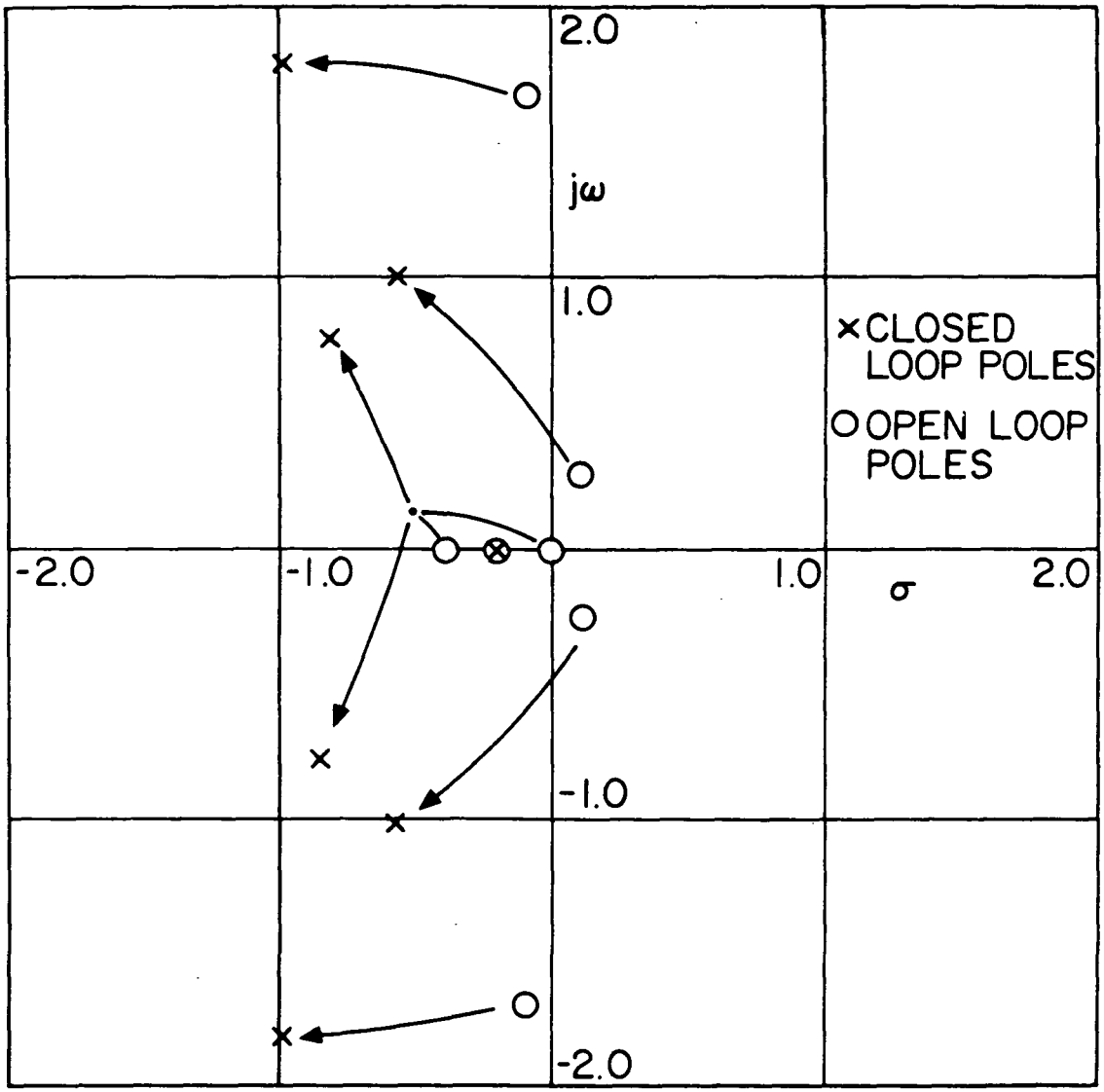

FIG. 3.1 Open-Loop and Closed-Loop Poles of the Longitudinal System

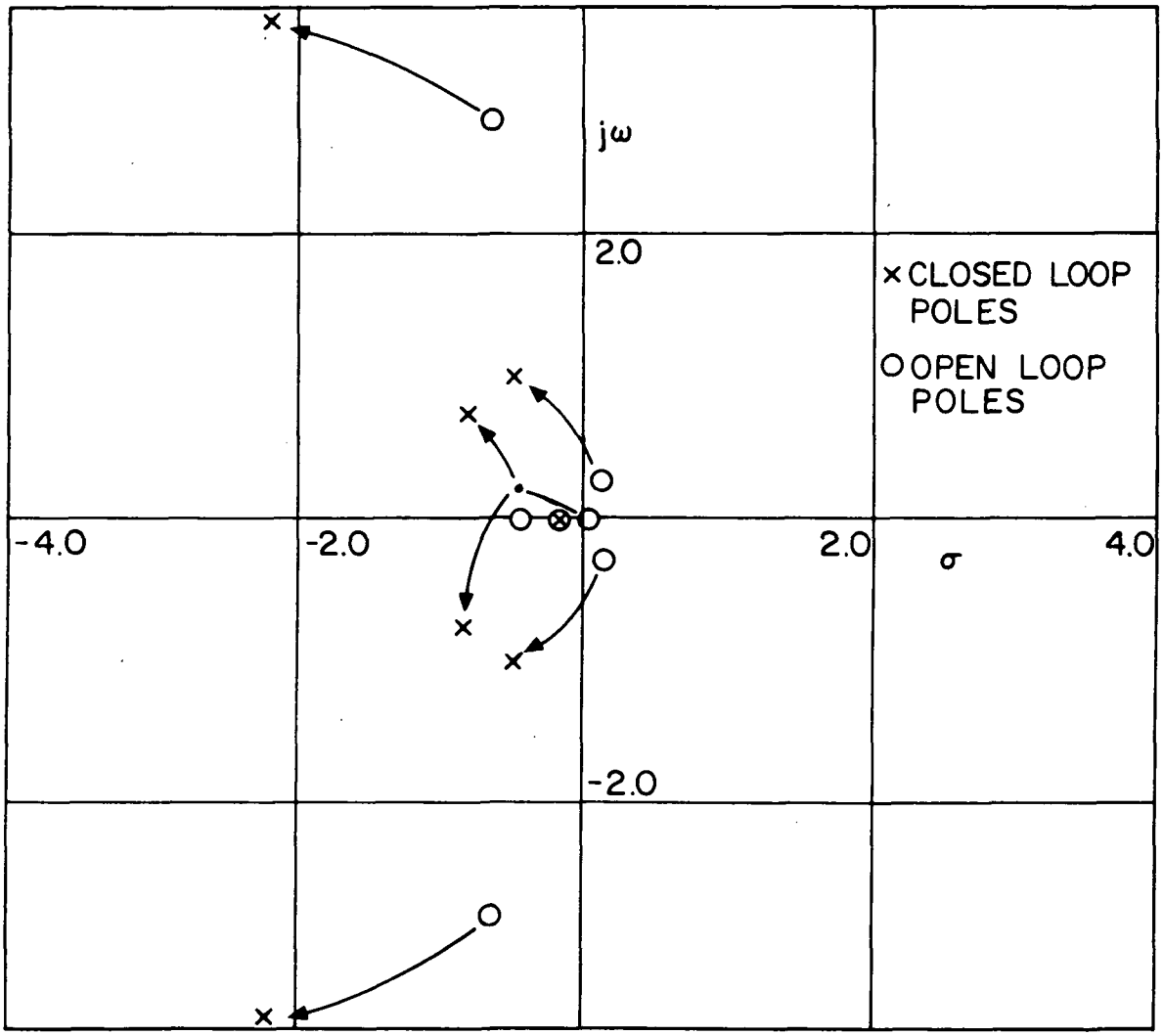

FIG. 3.2 Open-Loop and Closed-Loop Poles of the Lateral System

Table III-2

RMS Response with Perfect State Information
(Wind RMS 7 m sec^{-1} longitudinal and lateral, correlation time 5 sec.)

Longitudinal System

System	Technique	θ_v	$\dot{\theta}_v$	x_v	$\dot{x}_v$	x_ℓ	$\dot{x}_\ell$	$u_1(\approx\theta_R)$
Decoupled	1	.00290	.00495	.0292	.0251	.0248	.0169	.00943
	2	.00331	.00601	.0383	.0297	.0223	.0183	.00948
Coupled	1	.00329	.00589	.0381	.0283	.0367	.0199	.0100
	2	.00366	.00682	.0453	.0324	.0351	.0211	.0101

Lateral System

System	Technique	Φ_v	$\dot{\Phi}_v$	y_v	$\dot{y}_v$	y_ℓ	$\dot{y}_\ell$	$u_2(\approx\Phi_R)$
Decoupled	1	.00291	.00697	.0300	.0251	.0209	.0141	.00936
	2	.00338	.00873	.0391	.0299	.0183	.0153	.00939
Coupled	1	.00335	.00831	.0389	.0290	.0346	.0177	.00989
	2	.00379	.00984	.0463	.0334	.0330	.0186	.00992

[Units in m , sec ; angles in rad]

Figure 3.1 shows how the poles of the longitudinal system move when the feedback gains of Table III-1 are used. The poorly damped complex pole pair becomes better damped and faster. The unstable complex pole pair becomes stable and the two real poles change into a complex pair. The pole at -.2 corresponds to the wind model and cannot be moved by feedback since wind velocity is external to the system. The eigenvalue identification was done using the eigenvectors given in Appendix A. A similar graph for the lateral system is shown in Figure 3.2.

The root-mean-square (RMS) response of the system is determined assuming perfect state information (B1, Chapter 15). Table III-2 shows the RMS values of the state and control variables when procedures (1) and (2) are used to find feedback gains on wind velocity. Also shown is the predicted performance when the gains from the decoupled systems are used with the coupled 14th order system. Procedure (2) gives a lower RMS value of the deviation in position of the hanging load though at the cost of higher RMS value of other state variables. The RMS errors are quite small for this strong gusty wind.

3.3 Filter Design and RMS Response with Filter-Controller

A filter is designed to estimate the state variables from noisy measurements of Table II-3. The sum of ground plus wind velocity can be measured by mounting velocity probes on the helicopter. However, it is not necessary to do so. The wind velocity can be estimated if all other state variables are observable from the measurements. We assume that velocity probes are not used and build a filter to estimate the state variables and the wind. If $\hat{\underline{x}}$ is the estimated value of $\underline{x}$, then the estimation equation for the longitudinal system is

$$\frac{d}{dt}\begin{bmatrix}\hat{\underline{x}}\\ \hat{V}_{w_x}\end{bmatrix} = \begin{bmatrix} F & \Gamma \\ 0 & -1/\tau_c \end{bmatrix}\begin{bmatrix}\hat{\underline{x}}\\ \hat{V}_{w_x}\end{bmatrix} + \begin{bmatrix} G \\ 0 \end{bmatrix} u + K\left[\underline{z}-H\hat{\underline{x}}\right] \tag{3.7}$$

where $\underline{z}$ and H are defined for the longitudinal and lateral systems in equation (2.25) and Table II-5. The 7×3 gain matrix K is given in Table III-3. We define $\tilde{x}$, the error in estimate of $\underline{x}$, thus

$$\tilde{\underline{x}} = \underline{x} - \hat{\underline{x}} \tag{3.8}$$

The RMS estimation errors and the poles of the estimate error equations, are shown in Table III-3.

Table III-3

Filters for Longitudinal and Lateral System

$\underline{x}$	$K_{longitudinal}$			$\underline{x}$	$K_{lateral}$		
θ_v	-.661	-.482	2.51	ϕ_v	-.670	-.733	3.37
$\dot{\theta}_v$	-1.61	-1.07	4.49	$\dot{\phi}_v$	-1.94	-1.92	7.65
x_v	-17.8	-.494	-35.0	y_v	18.6	1.42	25.0
$\dot{x}_v$	-.626	2.60	-26.7	$\dot{y}_v$	3.08	-1.66	21.6
x_ℓ	-16.9	3.58	-19.5	y_ℓ	16.6	-3.68	11.1
$\dot{x}_\ell$	-5.13	-.142	-9.25	$\dot{y}_\ell$	5.47	.544	6.12
V_{w_x}	257	203	-717	V_{w_y}	-204	-245	796
$\underline{z}^T$	$[\theta_m$	θ_{ℓ_m}	$\theta_v]$	$\underline{z}^T$	$[\phi_m$	ϕ_{ℓ_m}	$\phi_v]$

Eigenvalues of the Estimate Error Equation (sec^{-1})

Longitudinal	$-1.1 \pm 2.5j$	$-.15 \pm .82j$	$-.34 \pm .19j$	-2.3
Lateral	$-1.7 \pm 3.9j$	$-.17 \pm .81j$	$-.33 \pm .23j$	-3.3

RMS Estimation Error

θ_v	$\dot{\theta}_v$	x_v	$\dot{x}_v$	x_ℓ	$\dot{x}_\ell$	V_{w_x}	ϕ_v	$\dot{\phi}_v$	y_v	$\dot{y}_v$	y_ℓ	$\dot{y}_\ell$	V_{w_y}
.0062	.0116	.232	.099	.205	.085	3.59	.0072	.0246	.21	.092	.187	.083	3.04

[Units in m , sec ; angles in radians]

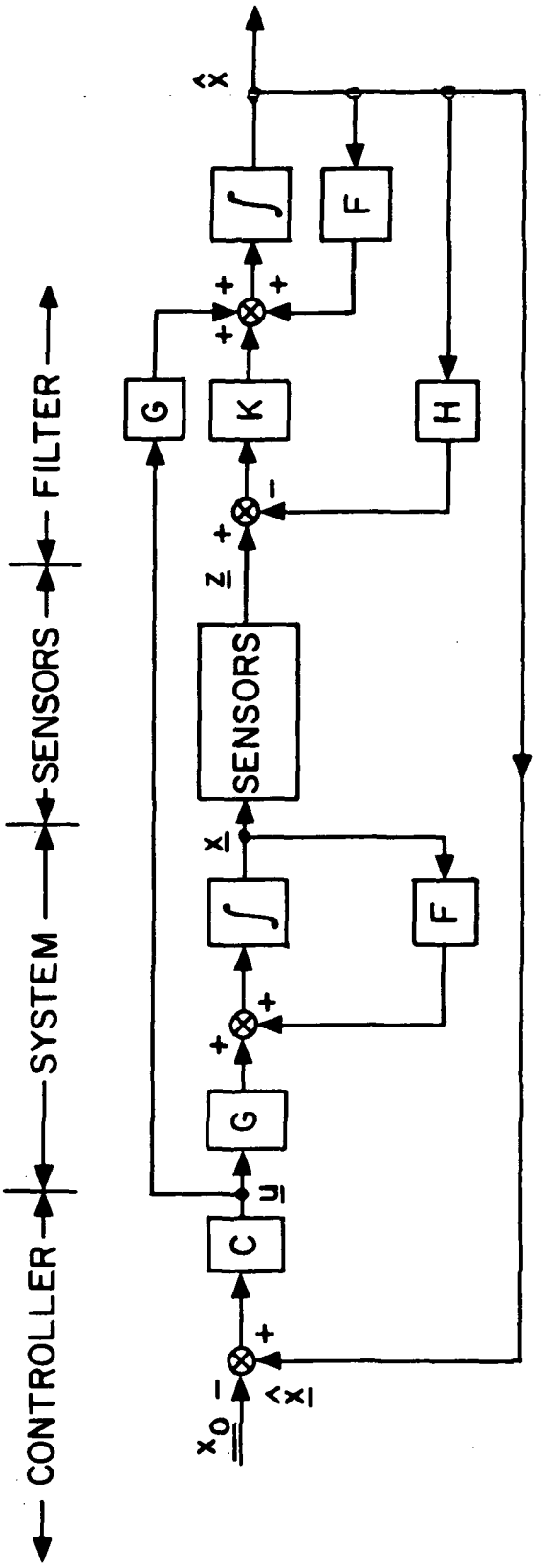

FIG. 3.3 System Implementation

Figure 3.3 shows how the system may be implemented. The complete system is divided into four parts: (a) controller, (b) system dynamics, (c) sensors, and (d) filter.

The filter-controller can be regarded as a multi-input multi-output compensator. The transfer function matrices of the compensators and the pole-zero locations are given in Appendix B. The compensators for both longitudinal and lateral systems have a pole in the right half plane. Some elements of the transfer function matrices also have a zero in the right half plane. Hence, these are nonminimum phase compensators.

The RMS response of the system is determined with the filter and the controller designed above in the presence of . 7 m sec^{-1} RMS longitudinal and lateral wind. Table III-4 summarizes the results for gain on wind from both techniques and also when the filter and controller gains from the decoupled systems are used on the coupled system.

Table III-4

RMS Response with Filter and Controller

(Wind 7 m sec^{-1} RMS longitudinal and lateral)

Longitudinal System

System	Technique	θ_v	$\dot{\theta}_v$	x_v	$\dot{x}_v$	x_ℓ	$\dot{x}_\ell$	$u_1(\approx\theta_R)$
Decoupled	1	.0341	.0736	.403	.313	.470	.241	.0247
	2	.0342	.0740	.403	.314	.468	.240	.0249
Coupled	1	.0355	.0771	.405	.320	.470	.242	.0253
	2	.0357	.0775	.405	.321	.469	.242	.0255

Lateral System

System	Technique	ϕ_v	$\dot{\phi}_v$	y_v	$\dot{y}_v$	y_ℓ	$\dot{y}_\ell$	$u_2(\approx\phi_R)$
Decoupled	1	.0327	.101	.340	.288	.394	.202	.0182
	2	.0328	.102	.339	.287	.393	.202	.0183
Coupled	1	.0339	.105	.340	.290	.394	.202	.0187
	2	.0341	.106	.340	.291	.393	.202	.0188

(Units in m , sec ; angles in radians)

There is considerable increase in RMS deviation of the hanging load position and control as compared to the case with perfect state information (see Table III-2). Nevertheless, the errors are still small for such a strong gusty wind. The coupled system gives nearly the same response.

3.4 Integral Feedback

The filter-controller of Sections 3.2 and 3.3 was designed assuming an exponentially correlated wind. In the presence of a steady wind, it produces a steady-state error. This steady-state error can be eliminated by the addition of integral feedback, which makes the position insensitive to steady disturbances or small changes in system parameters.

We add a new state variable, ξ , defined in equation (3.1) to the longitudinal system giving

$$\frac{d}{dt}\begin{bmatrix}\underline{x}\\ \hline \xi\end{bmatrix} = \begin{bmatrix}F & 0\\ \hline T & 0\end{bmatrix}\begin{bmatrix}\underline{x}\\ \hline \xi\end{bmatrix} + \begin{bmatrix}G\\ \hline 0\end{bmatrix}\underline{u} + \begin{bmatrix}\Gamma\\ \hline 0\end{bmatrix} V_{w_x} \tag{3.9}$$

If,
$$\underline{u} = G_{\underline{x}} + c_{\xi}\,\xi \tag{3.10}$$

$$\frac{d}{dt}\begin{bmatrix}\underline{x}\\ \hline \xi\end{bmatrix} = \begin{bmatrix}F+GC & Gc_{\xi}\\ \hline T & 0\end{bmatrix}\begin{bmatrix}\underline{x}\\ \hline \xi\end{bmatrix} + \begin{bmatrix}\Gamma\\ \hline 0\end{bmatrix} V_{w_x} \tag{3.11}$$

The gains can be chosen either by quadratic synthesis or by a mixture of quadratic synthesis and pole assignment. If the closed loop system is stable and V_{w_x} is a constant wind, then x_ℓ can be brought to zero in the steady state, by proper choice of c_{ξ} .

A filter is designed to estimate the state variable $\underline{x}$. The new state variable, ξ , can be estimated by using one of the two methods given here.

(i) $$\dot{\hat{\xi}} = \hat{x}_\ell \tag{3.12}$$

or (ii) $$\dot{\hat{\xi}} = z_x \equiv x_\ell + v_\ell \tag{3.13}$$

With perfect state information the two methods are the same.

Table III-5

Integral Control for the Longitudinal System

Controller: $J = \frac{1}{2} E\left\{\left(\frac{\theta_v}{2}\right)^2 + \left(\frac{x_v}{2}\right)^2 + \left(\frac{x_\ell}{1}\right)^2 + \left(\frac{\xi}{10}\right)^2 + \left(\frac{\theta_R}{1}\right)^2\right\}$ s.s.

c_{θ_v}	$c_{\dot{\theta}_v}$	c_{x_v}	$c_{\dot{x}_v}$	c_{x_ℓ}	$c_{\dot{x}_\ell}$	c_ξ
-1.31	-.273	.156	.166	-.0171	.169	.01

Filter:

$$\underline{x}^T = [\theta_v \quad \dot{\theta}_v \quad x_v \quad \dot{x}_v \quad x_\ell \quad \dot{x}_\ell] \qquad \underline{z}$$

$$K^T = \begin{bmatrix} -.888 & -2.64 & -17.8 & .598 & -17.1 & -4.58 \\ -.631 & -1.69 & -.483 & 3.31 & 3.39 & 2.24 \\ 3.10 & 7.18 & -34.9 & -29.7 & -18.7 & -10.7 \end{bmatrix} \begin{bmatrix} \theta_m \\ \theta_{\ell m} \\ \theta_v \end{bmatrix}$$

RMS State and Control

Wind State		θ_v	$\dot{\theta}_v$	x_v	$\dot{x}_v$	x_ℓ	$\dot{x}_\ell$	ξ	$u_1 (\approx \theta_R)$
(a)	PSI*	.00831	.0232	.0476	.0651	.0571	.0417	.233	.0122
	Filter	0.344	.0741	.401	.337	.481	.268	2.42	.0268
(b)	PSI	.0179	0.0	.0398	0.0	0.0	0.0	1.78	.00926
	Filter	.0378	.0704	.400	.330	.478	.264	2.99	.0256

(a) Wind with 19.6 m^2 sec^{-1} spectral density and small correlation time.

(b) 7.0 m sec^{-1} RMS steady wind

* Perfect State Information

Table III-6

Integral Control for the Lateral System

Controller: $J = \frac{1}{2} E\left\{\left(\frac{\phi_v}{2}\right)^2 + \left(\frac{y_v}{2}\right)^2 + \left(y_\ell\right)^2 + \left(\frac{\eta}{10}\right)^2 + \left(\frac{\phi_R}{11}\right)^2\right\}$ s.s.

c_{ϕ_v}	$c_{\dot{\phi}_v}$	c_{y_v}	$c_{\dot{y}_v}$	c_{y_ℓ}	$c_{\dot{y}_\ell}$	c_η
-.855	-.125	-.149	-.138	.0120	-.169	-.01

Filter:

$$\underline{x}^T = [\phi_v \quad \dot{\phi}_v \quad y_v \quad \dot{y}_v \quad y_\ell \quad \dot{y}_\ell] \qquad \underline{z}$$

$$K^T = \begin{bmatrix} -1.30 & -6.12 & 18.6 & 1.85 & 16.8 & 4.85 \\ -1.37 & -5.99 & 1.43 & -2.82 & -3.46 & -.087 \\ 5.76 & 23.7 & 24.9 & 26.2 & 10.3 & 8.53 \end{bmatrix} \begin{bmatrix} \phi_m \\ \phi_{\ell m} \\ \phi_v \end{bmatrix}$$

RMS State and Control

Wind State		ϕ_v	$\dot{\phi}_v$	y_v	$\dot{y}_v$	y_ℓ	$\dot{y}_\ell$	η	$u_2(\approx\phi_R)$
(a)	PSI*	.0127	.0602	.0492	.078	.0549	.0411	.0219	.0128
	Filter	.0352	.116	.345	.321	.413	.233	2.05	.0220
(b)	PSI	.0181	0.0	.0398	0.0	0.0	0.0	1.67	.00924
	Filter	.0373	.0988	.343	.312	.409	.229	2.64	.0201

(a) Wind with 19.6 $m^2 sec^{-1}$ spectral density and small correlation time.

(b) 70 m sec^{-1} RMS steady wind

* Perfect State Information

Table III-5 shows the controller gains (obtained using quadratic synthesis) and filter gains for the longitudinal system. The filter was designed for a wind with 19.6 $m^2 sec^{-1}$ spectral density and small correlation time. This table also shows the RMS state and control in two different wind states: (a) wind with 19.6 $m^2 sec^{-1}$ spectral density and small correlation time (approximated "white"), and (b) 7.0 m sec^{-1} RMS steady wind. With filter the second method is used to estimate the augmented state variable.

The response is excellent with perfect state information. In case (b) the root mean square (RMS) value of deviation in position of the hanging load is zero. With noisy measurements and a filter the RMS values of state and control variables increase but are quite reasonable.

Similar data for the lateral systems are given in Table III-6.

With integral control in the presence of steady wind disturbance, the wind velocity is not required for feedback and is not estimated. The above filter is designed to estimate other state variables. This filter is not optimal, since for a system in which the states are coupled through state transition, noise distribution or measurement distribution matrix the equations governing optimal state estimates are coupled.

3.5 Summary

An autopilot was designed for precision hover of a hanging load over a desired point. Satisfactory performance is obtained using a reasonable amount of control.

The response is much better using the assumption of perfect state information (ideal case) than with noisy measurements and optimal filter. To improve performance significantly, it is necessary to have better measurements. Integral control will prove useful only if better measurements are available.

Chapter IV

MOVING THE HANGING LOAD OVER SHORT DISTANCES

4.1 Introduction

In many applications of interest the load has to be carried over short distances. In such cases the time spent near the terminal points is large compared to travel time and it is advantageous to carry the load without retracting the cables even if it requires traveling only at moderate speeds. We assume that the helicopter travels sufficiently slowly that aerodynamic instabilities (coupled yaw and lateral pendulum motions) of the cable-load combination do not arise.

In general the transfer is carried out in four stages: (a) zero velocity to cruise velocity at approximately constant acceleration, (b) cruise at constant velocity, (c) cruise velocity to zero velocity at constant deceleration, and (d) precision hover. For very short distances the cruise phase may be absent.

In what follows we present a general scheme for tranferring the system from any state to hover at the origin of the coordinate system. Autopilot modes are chosen depending on the location of the system in state space. There are four possible modes: Acceleration, cruise, deceleration, and hover. At a switch curve the autopilot shifts from one mode to another and the system experiences a transient. We first discuss the mode selection logic and then the autopilot logic for each mode.

4.2 Mode Selection

The longitudinal system has six state variables. If one or more of the state variables θ_v, $\dot{\theta}_v$, θ_ℓ, and $\dot{\theta}_\ell$ has large initial values, the system is placed in a stabilization mode. In this mode the position and velocity of the helicopter are not controlled but the pitch angle, the load cable inclination angle, and the corresponding angular rates are reduced to low values. It is necessary to do this for a simple switching diagram because acceleration or velocity

commands might otherwise produce unacceptable angular deviations for a short period of time. Thus as a starting condition we have small θ_v , $\dot{\theta}_v$, θ_ℓ , and $\dot{\theta}_\ell$, and any x_v and $\dot{x}_v$.

The switching diagram is shown in Figure 4.1 in the x_v , $\dot{x}_v$ space. The cruise velocity is fixed at v_{max} and the commanded acceleration at $\pm a_{max}$. Roughly, the reduced state space (x_v , $\dot{x}_v$ space) is divided into four regions. The commanded mode is a function of x_v and $\dot{x}_v$ as follows:

If $|\dot{x}_v| > v_h$, $|x_v| > x_h$, and

$\dot{x}_v^2 \text{sgn}(\dot{x}_v) < -2ax_v$ and $\dot{x}_v < v_{max}$ Acceleration Mode

and $\dot{x}_v > v_{max}$ Deceleration Mode

and $\dot{x}_v = v_{max}$ Cruise Mode

$\dot{x}_v^2 \text{sgn}(\dot{x}_v) > -2ax_v$ and $\dot{x}_v > -v_{max}$ Deceleration Mode

and $\dot{x}_v > -v_{max}$ Acceleration Mode

If $|\dot{x}_v| \leq v_h$ and $|x_v| \leq x_h$ Hover Mode.

(4.1)

The figure shows the details of the switching logic. It takes some time for the system to go into the new mode after mode switching is commanded. Therefore the system should be commanded to go into the new mode before it approaches the mode switching boundary of (4.1). The dotted lines in the diagram are the boundaries where the new mode is commanded. The switching curves for bang-bang type control have some dead space around them to avoid the problem of chattering. The dotted lines around the mode switching curves do not represent dead space alone. This is the space required for mode change to take place.

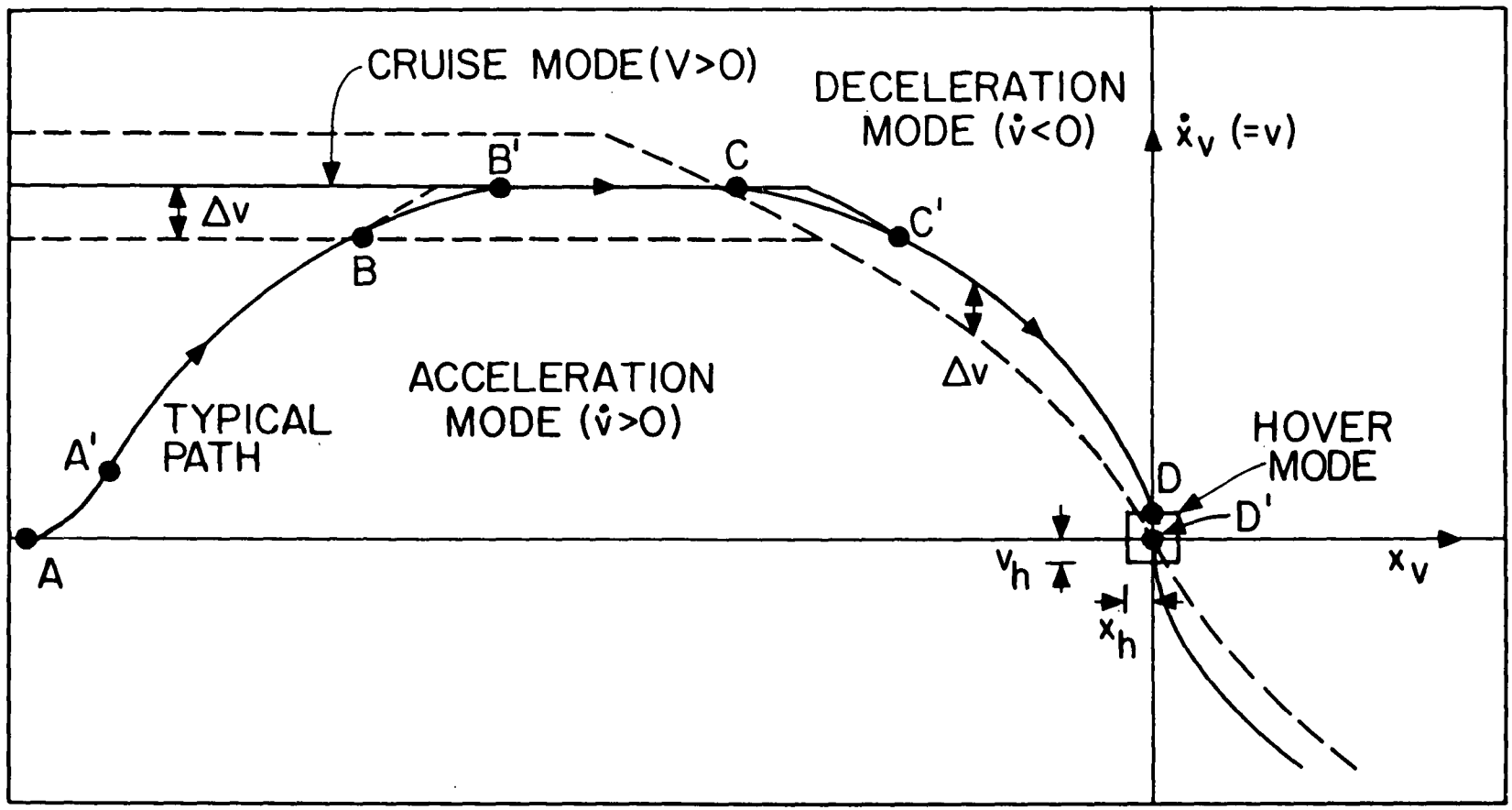

FIG. 4.1 Mode Selection Logic

An example trajectory is shown. At the starting point, A , with the helicopter standing still, acceleration is commanded. The aircraft travels to point A' before constant acceleration is achieved. The Cruise Mode is commanded at B and the helicopter travels to point B' before the velocity is constant at v_{max} . This is followed by the Deceleration Mode (C-C'-D) and the Hover Mode (D-D') .

For the system under consideration the following parameters are chosen

$$
\begin{aligned}
v_{max} &= 15 \text{ m sec}^{-1} \\
\Delta v &= 2 \text{ m sec}^{-1} \\
a_{max} &= 1 \text{ m sec}^{-2} \\
x_h &= 1.0 \text{ m} \\
v_h &= 1.0 \text{ m sec}^{-1}
\end{aligned}
\tag{4.2}
$$

4.3 Command Generating Model

The command generating model produces commands to switch mode or change trim state with acceptable transient response. The desired changes are smoothed out so that the system can follow them with reasonable state variable deviations and control. The structure of the model depends upon the commands desired and the kind of transient response desired. In the model designed here, constant acceleration or velocity can be commanded. If a_d is the desired acceleration, the command velocity, v_c , and commanded acceleration, a_c , are given by

$$\dot{v}_c = a_c \tag{4.3}$$

$$\dot{a}_c = \frac{1}{\tau} (a_d - a_c) \tag{4.4}$$

Follower

For velocity or acceleration commands, we are not interested in controlling position, so the longitudinal equations of motion can be written in terms of only five state variables, θ_v, $\dot{\theta}_v$, $\dot{x}_v$, θ_ℓ, and $\dot{\theta}_\ell$ as shown in Appendix D. The controller can follow a constant velocity or acceleration command in the "steady state". In this "steady state", $\dddot{x}$ (rate of change of acceleration), $\dddot{\theta}_v$ and $\dddot{\theta}_\ell$ are zero. Differentiating the state equations twice and then once gives

$$\ddot{\theta}_v = \ddot{\theta}_\ell = 0 \tag{4.5}$$

and

$$\begin{bmatrix} \dot{\theta}_v \\ \dot{\theta}_\ell \end{bmatrix}_s = - \begin{bmatrix} .000254 \\ .000262 \end{bmatrix} a_c \tag{4.6}$$

Now the state variables and the control variable are proportional to a_c and v_c in this "steady-state":

$$\begin{bmatrix} \theta_v \\ \dot{\theta}_v \\ \dot{x}_v \\ \theta_\ell \\ \dot{\theta}_\ell \end{bmatrix}_s = \begin{bmatrix} -.102 & -.000254 \\ -.000254 & 0.0 \\ 0.0 & 1.0 \\ -.102 & -.000262 \\ -.000262 & 0.0 \end{bmatrix} \begin{bmatrix} a_c \\ v_c \end{bmatrix} = M\underline{y}_c \tag{4.7}$$

$$u_s = -.0000158\ a_c - .00132\ v_c = N\underline{y}_c \tag{4.8}$$

The desired control law is

$$u = u_s + C(\underline{x} - \underline{x}_s) \tag{4.9}$$

The gains C are given in Appendix D.

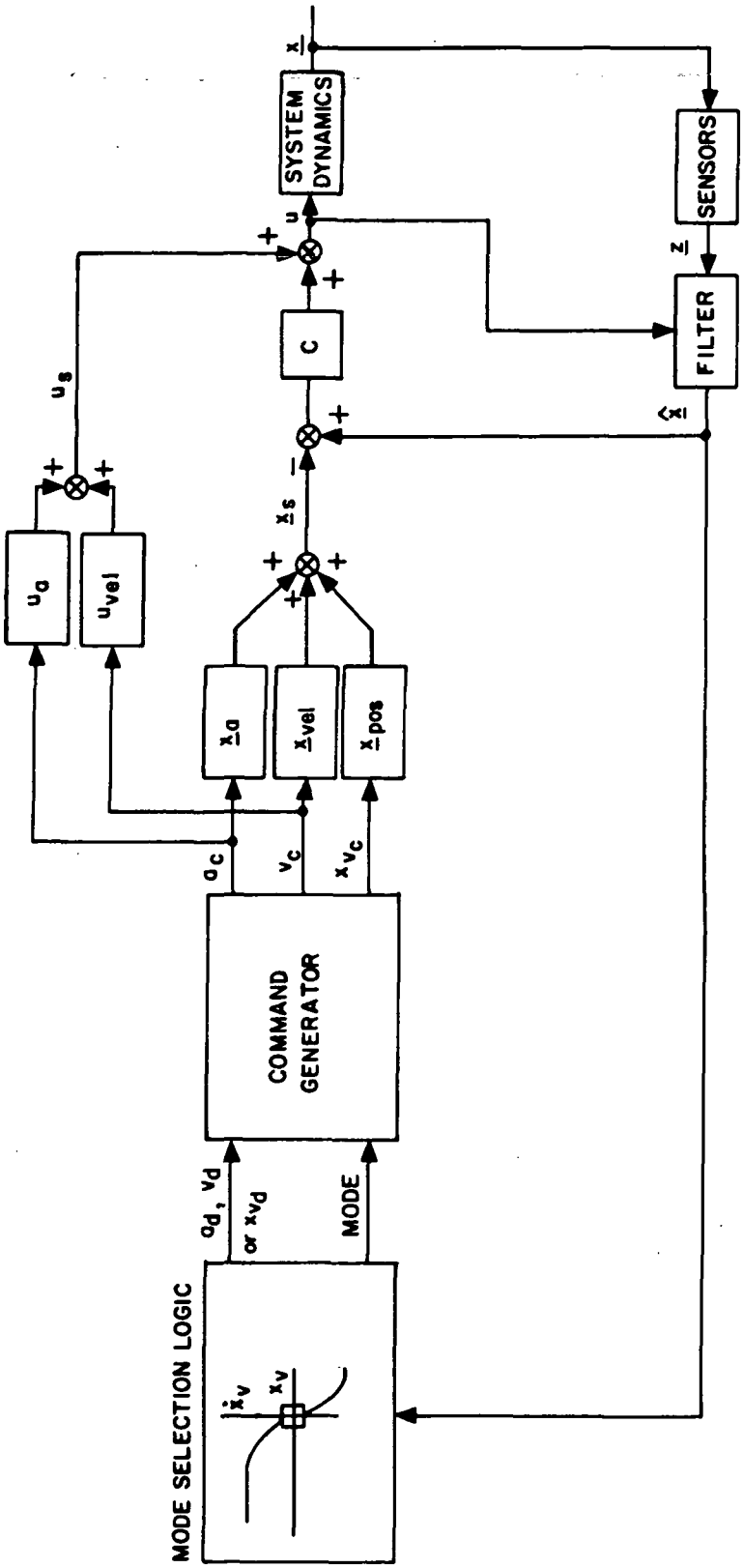

FIG. 4.2 Implementation of Mode Switching Logic

4.4 Transient Response

The transient response of the system was determined at mode switching. The following four cases were considered with the time constant of the command generating filter equal to 2 sec:

(a) Switching from hover to constant acceleration mode (Figure 4.3)

(b) Switching from constant acceleration mode to constant velocity mode (Figure 4.4)

(c) Switching from constant velocity mode to constant deceleration mode (Figure 4.5)

(d) Switching from constant acceleration to constant deceleration mode (Figure 4.6)

Good response was obtained in all cases as shown in figures (4.3) to (4.6). The closed loop frequency associated with pitch angle changes is higher than those associated with changes in inclination of the load cable or velocities of the vehicle and the hanging load. Thus after a mode is commanded, the pitch angle starts changing away from its previous trajectory first. The large transients in the rotor tilt in the beginning are due to fast changes in pitch angle and pitch rate. Notice that the initial transient response of the longitudinal tilt of the rotor NFP in figure 4.4 is similar to figure 4.5 (both involving a -1 m sec^{-2} change in commanded acceleration) and is "negative" of figure 4.3 (involving a 1 m sec^{-2} change in commanded acceleration).

In all cases the maximum rotor tilt in the longitudinal direction (control) was less than 2° (the maximum control authority is about 12°), while the pitch angle never exceeded 8° (the nominal "steady state" pitch angle in acceleration or deceleration mode is about 5.7°). Switching from constant deceleration to constant acceleration produced the largest transient.

4.5 Summary

It is possible to move hanging loads over short distances safely and efficiently without retracting the cables. The cable-load configuration

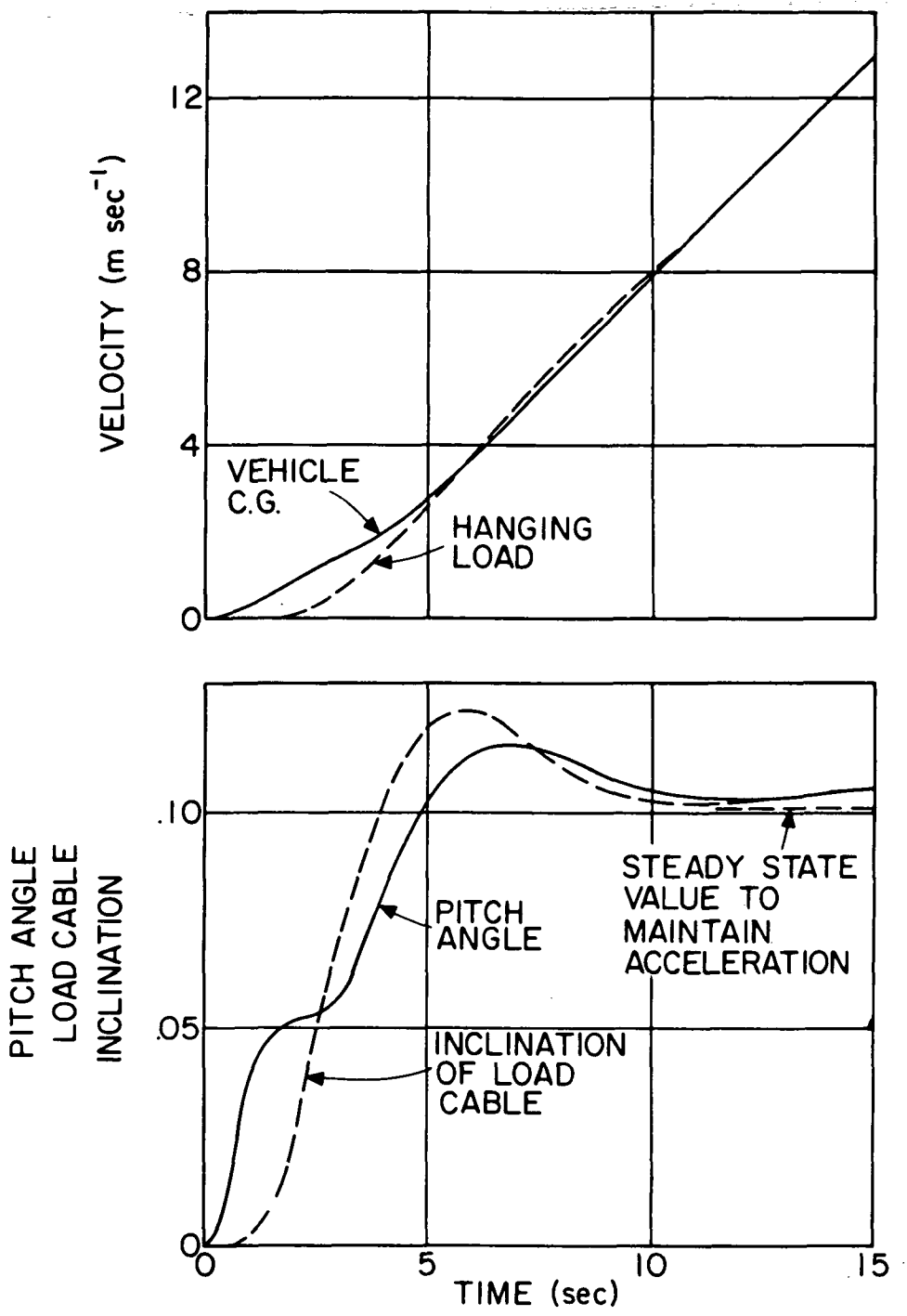

FIG. 4.3 Transition from Hover to Constant Acceleration Mode

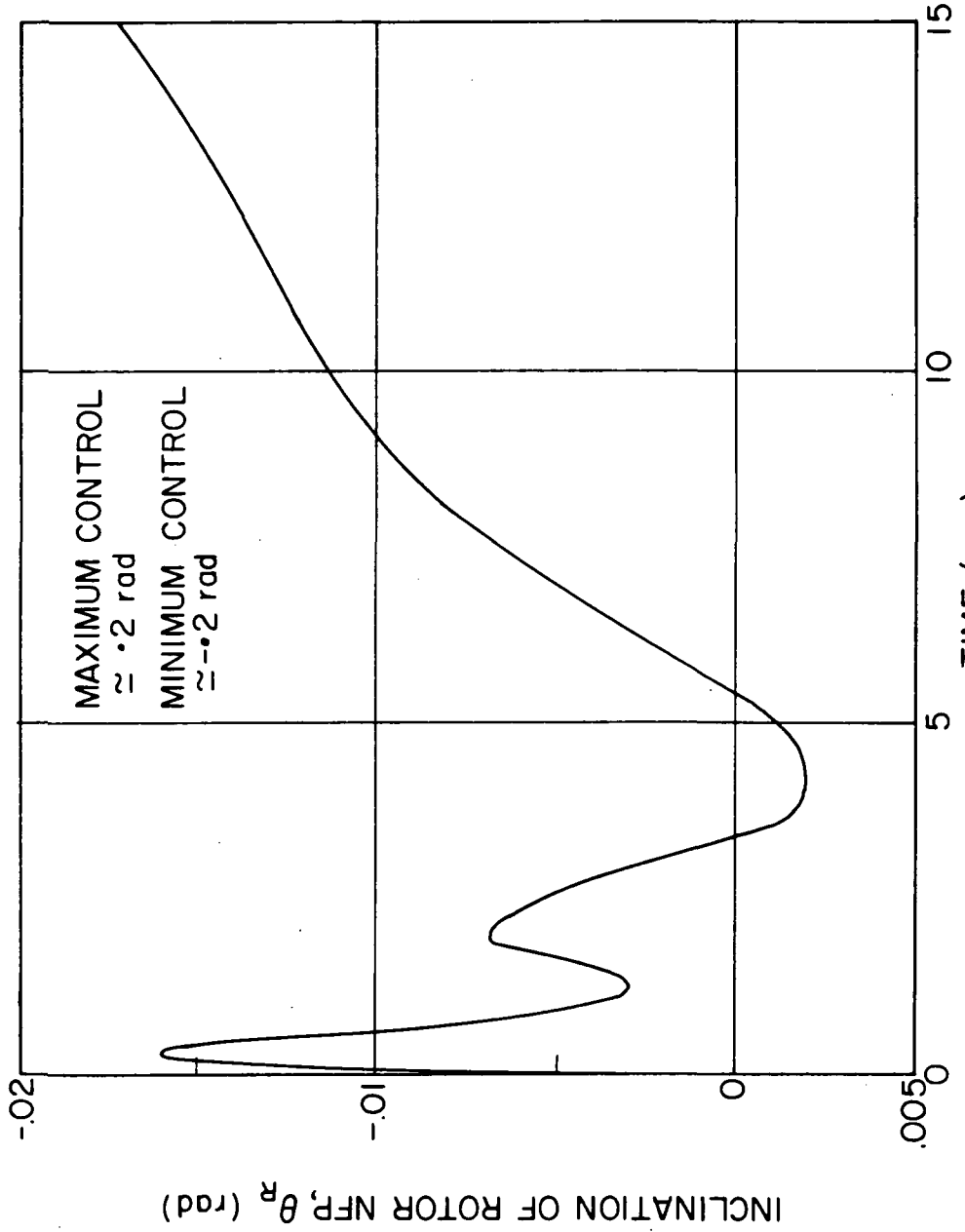

FIG. 4.3 (contd.) Transition from Hover to Constant Acceleration Mode

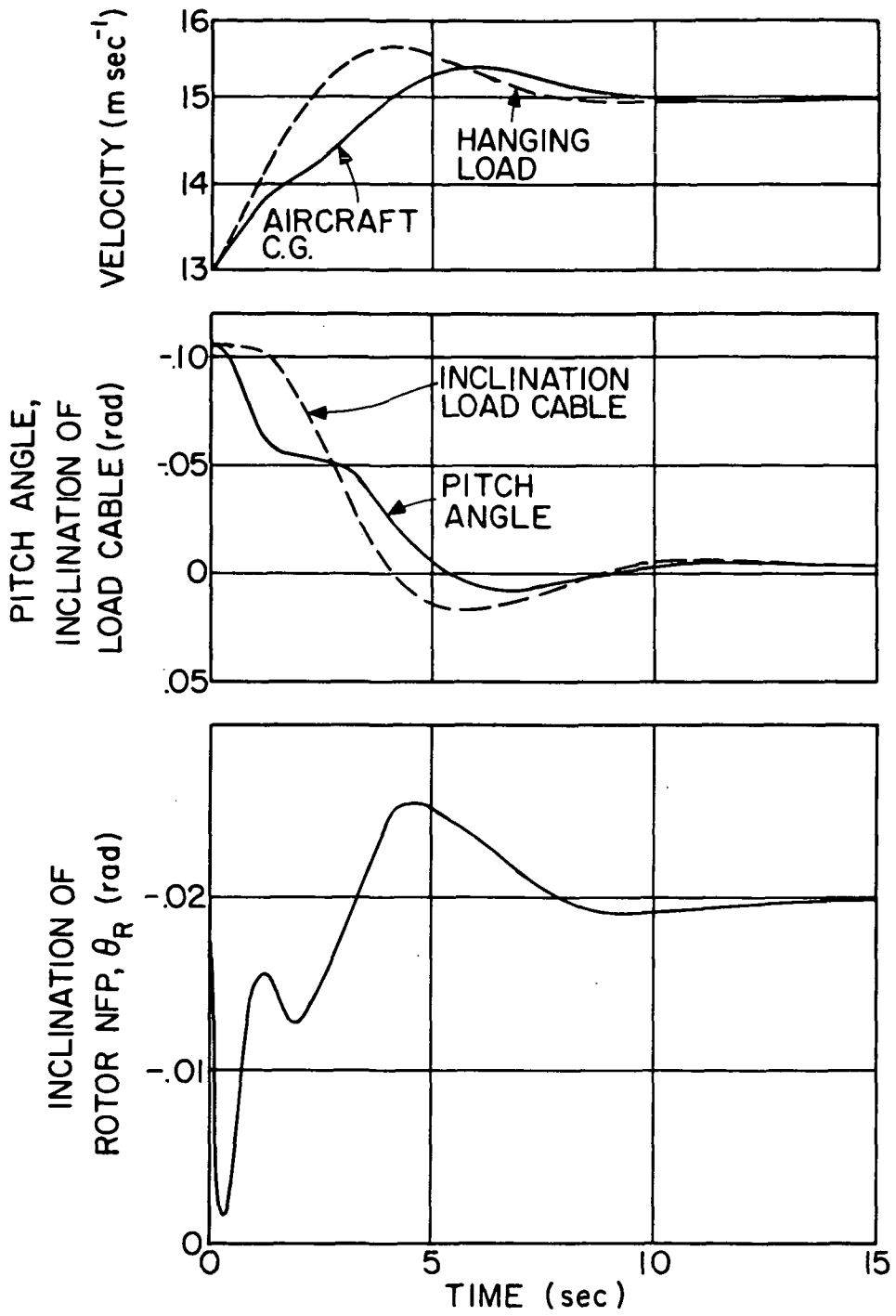

FIG. 4.4 Transition from Constant Acceleration to Constant Velocity Mode

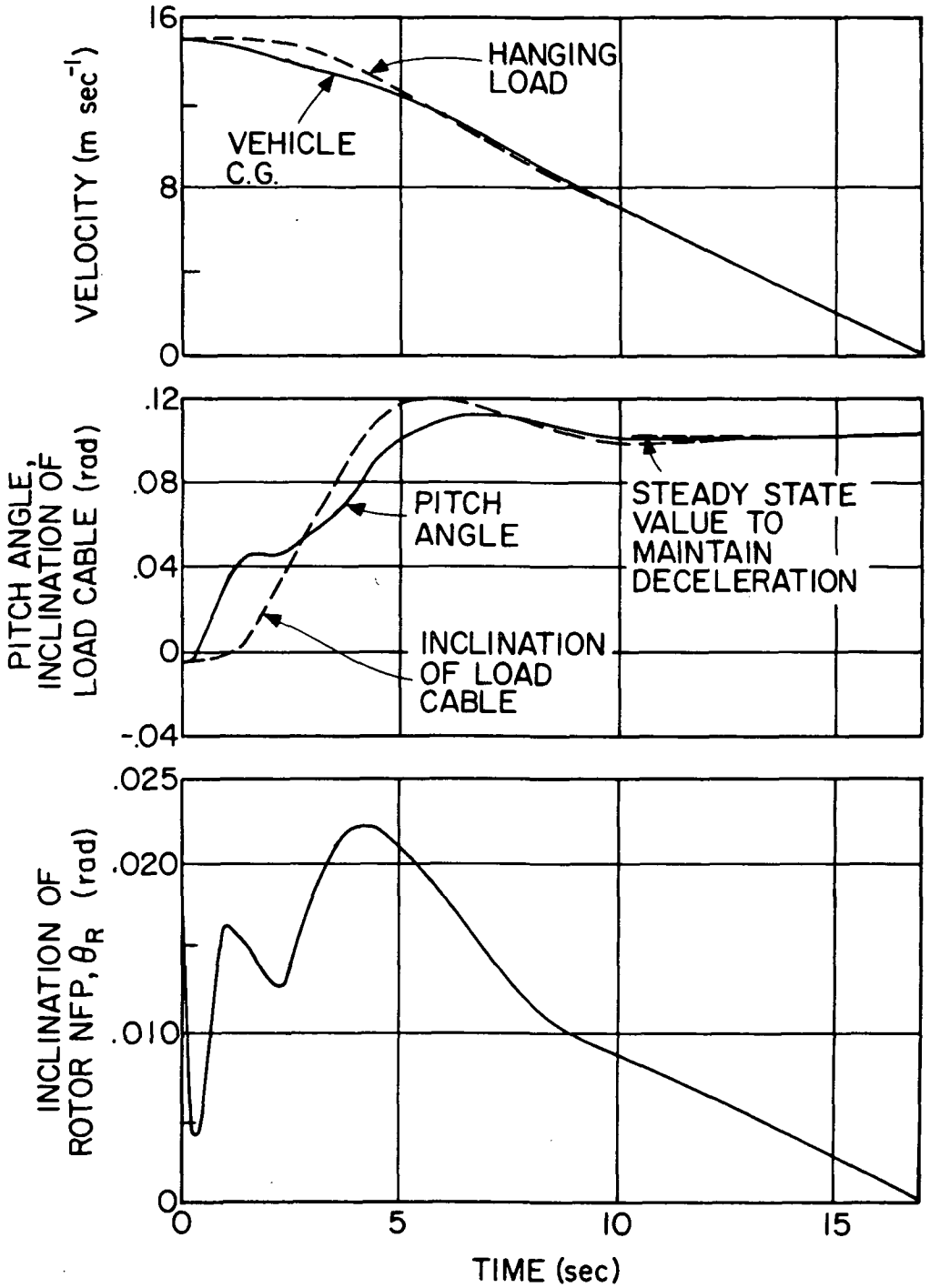

FIG. 4.5 Transition from Constant Velocity to Constant Deceleration Mode

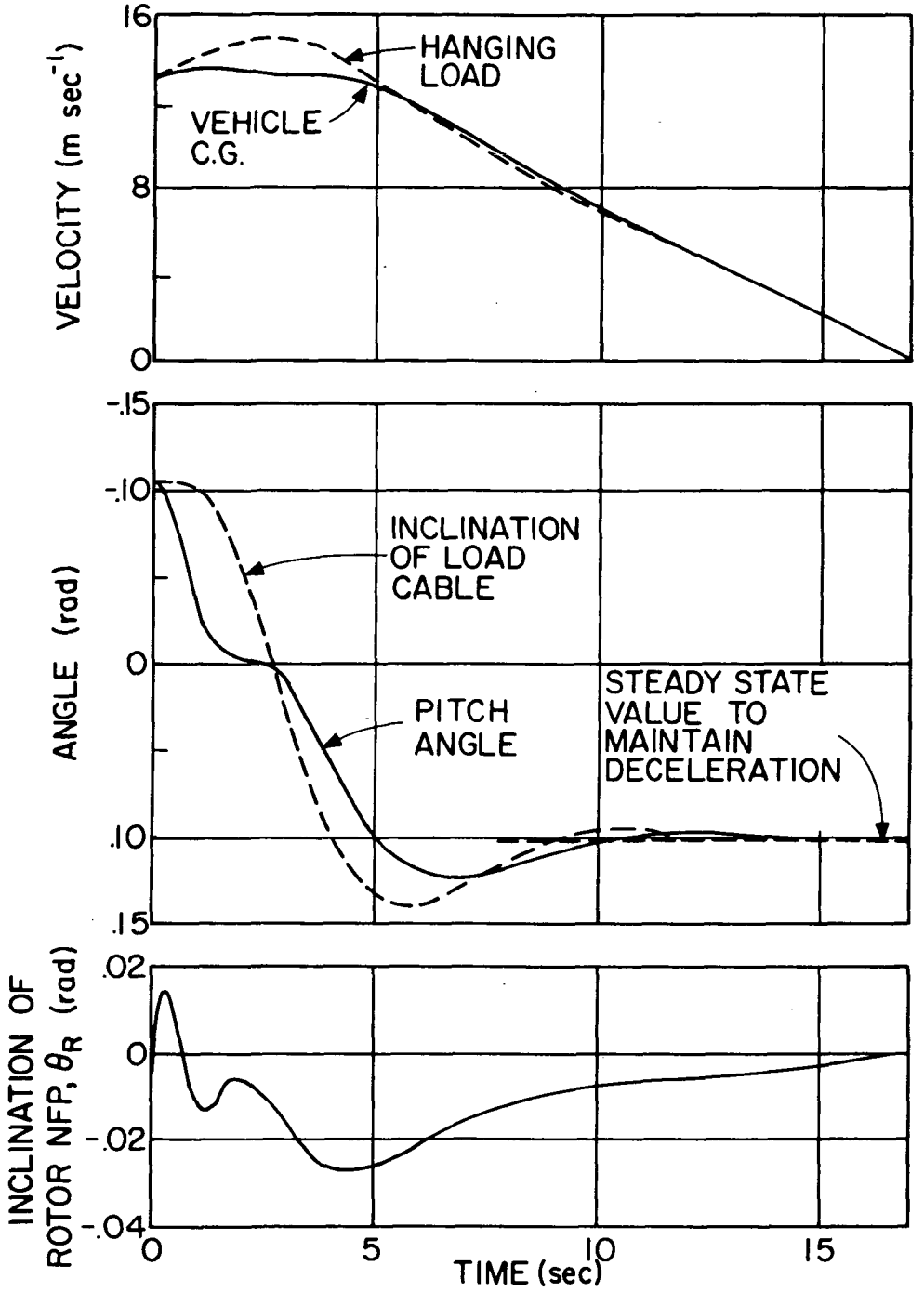

FIG. 4.6 Transition from Constant Acceleration to Constant Deceleration Mode

must be designed so that aerodynamic instabilities do not occur at velocities less than or equal to the cruise velocity. Studies by Gable and Wilson [G1] show that most practical hanging loads can be made aerodynamically stable up to a reasonable speed. Some thoeretical studies [P1] and experiments with one body shape and cable configuration [E1] point to the contrary. However, these latter studies assume that the aircraft moves at constant speed and neglects the effect of the hanging load on the vehicle. This coupling is not negligible for modern crane helicopters and heavy lift helicopters, where the mass of the helicopter is comparable to that of the payload.

Chapter V

PERFORMANCE UNDER OFF-DESIGN CONDITIONS

5.1 Introduction

In operation some of the parameters will differ from the values used in designing the control system, e.g., in off-loading container ships, all containers may not have the same mass (change in γ) or location of the center of mass (change in ℓ). In addition, the values of some of the system parameters may not be accurately known. Therefore it is prudent to study the performance of the system when the gains for the design condition are used with a different configuration.

We have shown that the decoupling approximation is quite good for the purpose of designing the controller and the filter and is reasonable for evaluating the performance. Also the behavior of the longitudinal and lateral systems is of the same character. Therefore it is sufficient to carry out a thorough investigation of the longitudinal system only.

5.2 System Definition Matrices

We believe the following four parameters are the most likely ones to change in normal operation:

(a) mass of the vehicle, because of varying amounts of fuel
(b) mass of the hanging load (or the ratio $\gamma = \frac{m_v+m_\ell}{m_v}$)
(c) the distance between the suspension point and the center of gravity of the hanging load
(d) drag coefficient on the hanging load

These parameters are changed one at a time and the matrices F, G, Γ, and H are computed. The mass of the vehicle is changed to 5000 kg and 7000 kg (nominal value 6000 kg), the mass of the hanging load is changed to 1000 kg and 3000 kg (nominal value 2000 kg), the length of the cable, ℓ, is changed to 10 m and 30 m (nominal value

20 m) and the drag coefficient on the load is increased and decreased by a factor of ten from its nominal value of .0026 sec^{-1}.

The open loop eigenvalues of the longitudinal system are shown in Table V-1. The character of the eigenvalues is the same. The mass of the hanging load and the length of the cable seem to be important parameters.

5.3 Closed Loop System

The nominal controller and filter gains obtained for the design configuration are used with the system matrices obtained for off-design conditions. Table V-2 shows the closed loop eigenvalues. The eigenvalues move but all the closed loop systems remain stable. The damping of all the roots is good except for one root pair for γ=1.1667 (1000 kg hanging load). Filter eigenvalues are shown in Table V-3. All filters remain stable and the poles do not move much. It seems that it is possible to use the design filter and controller gains even with these wide fluctuations in parameters.

Root mean square (RMS) state and control response in the presence of a 7 m sec^{-1} RMS exponentially correlated wind (correlation time 5 sec) are shown in Table V-4 with perfect state information (ideal case) and in Table V-5 with noisy measurements and filter with fixed gains. Except for the case with increased drag coefficient on the hanging load, the state and control responses do not deteriorate appreciably. With increased drag coefficient (last case) the RMS value of the deviation in the position of hanging load increases from .033 m to .481 m with perfect state information (PSI) and from .47 m to .77 m with noisy measurements and filter. We achieve suboptimal performance by using controller and filter gains which are optimal only under design conditions. The performance can be improved by choosing a different set of gains for each configuration but it does not seem necessary. In some instances this suboptimal performance is superior to the design case because those configurations are more favorable than the design configuration.

Table V-1

Open Loop Eigenvalues Under Off-Design Conditions

m_v	$\gamma = \frac{m_v + m_\ell}{m_v}$	ℓ	$(\gamma-1)\sigma_5$	Open Loop Eigenvalues of the Longitudinal Model				
6000	1.33	20	.0026**	-.11 $\pm$ 1.7j	.095 $\pm$ .26j	-.40	0.0	-.20
6000	1.33	10	.0026	-.14 $\pm$ 2.3j	.0091 $\pm$ .33j	-.18	0.0	-.20
6000	1.33	30	.0026	-.097 $\pm$ 1.4j	.12 $\pm$ .26j	-.48	0.0	-.20
5000	1.33	20	.0026	-.14 $\pm$ 1.7j	.097 $\pm$ .27j	-.45	0.0	-.20
7000	1.33	20	.0026	-.098 $\pm$ 1.7j	.095 $\pm$ .25j	-.37	0.0	-.20
6000	1.50	20	.0026	-.13 $\pm$ 2.0j	.093 $\pm$ .25j	-.37	0.0	-.20
6000	1.77	20	.0026	-.087 $\pm$ 1.3j	.10 $\pm$ .29j	-.47	0.0	-.20
6000	1.33	20	.00026	-.11 $\pm$ 1.7j	.098 $\pm$ .26j	-.40	0.0	-.20
6000	1.33	20	.026	-.11 $\pm$ 1.7j	.074 $\pm$ .23j	-.38	0.0	-.20

* Drag Coefficient on Hanging Load

** Design Condition

[Units in kg, m, sec]

Table V-2

Closed Loop Eigenvalues Under Off-Design Conditions Using Design Feedback Gains

m_v	$\gamma = \frac{m_v + m_\ell}{m_v}$	ℓ	$(\gamma-1)\sigma_5$*	Closed Loop Eigenvalues of the Longitudinal System			
6000	1.33	20	.0026**	-.99 ± 1.8j	-.84 ± .78j	-.58 ± 1.0j	-.20
6000	1.33	10	.0026	-1.1 ± 2.3j	-.41 ± .60j	-.90 ± 1.3j	-.20
6000	1.33	30	.0026	-.89 ± 1.6j	-1.1 ± .51j	-.41 ± 1.1j	-.20
5000	1.33	20	.0026	-.79 ± 1.7j	-1.1 ± .76j	-.55 ± .94j	-.20
7000	1.33	20	.0026	-1.0 ± 1.9j	-.82 ± .69j	-.52 ± 1.1j	-.20
6000	1.50	20	.0026	-.81 ± 2.2j	-1.5 ± .30j	-.42 ± .81j	-.20
6000	1.77	20	.0026	-1.3 ± 1.7j	-.67 ± .54j	-.19 ± 1.2j	-.20
6000	1.33	20	.00026	-.96 ± 1.8j	-.91 ± .75j	-.54 ± 1.0j	-.20
6000	1.33	20	.026	-.96 ± 1.8j	-.88 ± .67j	-.58 ± 1.1j	-.20

* Drag Coefficient on Hanging Load

** Design Condition

[Units in kg, m, sec]

Table V-3

Eigenvalues of the Estimate Error Equation

[Off Design Parameters and Design Filter Gains]

m_v	$\gamma = \frac{m_v + m_\ell}{m_v}$	ℓ	$(\gamma-1)\sigma_5^*$	Eigenvalues of Estimate Error Equation (Longitudinal)			
6000	1.33	20	.0026**	$-1.1 \pm 2.5j$	$-.15 \pm .82j$	$-.34 \pm .19j$	-2.3
6000	1.33	10	.0026	$-1.3 \pm 2.8j$	$-.29 \pm .86j$	$-.33 \pm .22j$	-1.8
6000	1.33	30	.0026	$-1.0 \pm 2.4j$	$-.10 \pm .79j$	$-.34 \pm .17j$	-2.5
5000	1.33	20	.0026	$-1.0 \pm 2.6j$	$-.15 \pm .82j$	$-.34 \pm .19j$	-2.6
7000	1.33	20	.0026	$-1.2 \pm 2.4j$	$-.15 \pm .82j$	$-.34 \pm .19j$	-2.0
6000	1.5	20	.0026	$-1.2 \pm 2.6j$	$-.15 \pm .88j$	$-.33 \pm .18j$	-2.1
6000	1.167	20	.0026	$-.97 \pm 2.3j$	$-.15 \pm .76j$	$-.34 \pm .19j$	-2.6
6000	1.33	20	.0026	$-.98 \pm 2.3j$	$-.14 \pm .76j$	$-.34 \pm .19j$	-2.6
6000	1.33	20	.026	$-.94 \pm 2.3j$	$-.19 \pm .71j$	$-.34 \pm .19j$	-2.6

[Units kg, m, sec]

* Drag coefficient on hanging load

** Design condition

Table V-4

RMS Response with Perfect State Information
Under Off-Design Conditions

[Wind RMS = 7 m sec^{-1}, Correlation Time = 5 sec]

				RMS State and Control						
m_v	$\gamma = \frac{m_v+m_\ell}{m_v}$	ℓ	$(\gamma-1)\sigma_5$ *	θ_v	$\dot{\theta}_v$	x_v	$\dot{x}_v$	x_ℓ	$\dot{x}_\ell$	$u_1(\approx\theta_R)$
6000	1.33	20	.0026**	.0029	.0050	.029	.025	.025	.017	.0094
6000	1.33	10	.0026	.0027	.0042	.025	.022	.031	.016	.0095
6000	1.33	30	.0026	.0032	.0054	.032	.027	.024	.018	.0094
5000	1.33	20	.0026	.0027	.0038	.021	.020	.038	.018	.0113
7000	1.33	20	.0026	.0032	.0059	.039	.029	.022	.018	.0081
6000	1.5	20	.0026	.0028	.0053	.034	.025	.021	.015	.0084
6000	1.167	20	.0026	.0035	.0051	.028	.029	.033	.021	.0107
6000	1.33	20	.00026	.0024	.0046	.033	.019	.033	.014	.0096
6000	1.33	20	.026	.0115	.0131	.197	.136	.481	.175	.0082

* Drag Coefficient on Hanging Load

** Design Condition

[Units in kg, m, sec; angles in rad]

Table V-5

RMS Response with Noisy Measurements and Filter
(Off-Design Conditions)

				RMS State and Control						
m_v	$\gamma = \frac{m_v + m_\ell}{m_v}$	ℓ	$(\gamma-1)\sigma_5^*$	θ_v	$\dot{\theta}_v$	x_v	$\dot{x}_v$	x_ℓ	$\dot{x}_\ell$	$u_1(x\theta_R)$
6000	1.33	20	.0026**	.0341	.0737	.404	.313	.470	.241	.0247
6000	1.33	10	.0026	.0244	.0599	.369	.259	.465	.217	.0234
6000	1.33	30	.0026	.0400	.0808	.428	.342	.484	.257	.0258
5000	1.33	20	.0026	.0368	.0788	.409	.330	.472	.244	.0260
7000	1.33	20	.0026	.0323	.0702	.400	.301	.469	.239	.0240
6000	1.5	20	.0026	.0273	.0671	.395	.277	.474	.224	.0226
6000	1.167	20	.0026	.0515	.0892	.467	.427	.494	.312	.0283
6000	1.33	20	.00026	.0508	.0883	.464	.422	.491	.307	.0282
6000	1.33	20	.026	.0593	.100	.561	.507	.770	.405	.0289

[Units in kg, m, sec ; angles in rad]

* Drag coefficient on hanging load

** Design condition

5.4 Summary

Satisfactory system behavior is obtained by using a fixed set of controller and filter feedback gains even though some of the system parameters vary within wide ranges. It seems unnecessary to use different gains with nominal changes in system parameters. However, a new set of gains would be required with a completely new system configuration or measurement system.

Chapter VI

SUMMARY

A mathematical model is developed for the motions of a hovering or slowly moving helicopter carrying a hanging load. Autopilot logic is designed for position-hold (hover), velocity-hold, and acceleration-hold.

It is shown that the longitudinal-lateral decoupling approximation is satisfactory for the purpose of autopilot design, except when a very tight control system is desired.

The root mean square (RMS) response of the controlled system is quite satisfactory in the presence of steady and gusty longitudinal and lateral winds. Further improvements in hovering accuracy could be attained by using a better measurement system, since substantially better performance is obtained using the assumption of perfect state information (ideal case) under design conditions.

The stability and performance of the system is examined for reasonable variations in system parameters. In no case does the system become unstable. The RMS response does not change appreciably except with a tenfold increase in drag coefficient on the hanging load. The behavior is satisfactory in all cases.

It is possible to move the hanging load over short distances rapidly without retracting the cables. This involves controlling the oscillations of the load while moving at a low velocity. In case of failure of the automatic control system the pilot can still control the system. Some load shapes and cable arrangements are aerodynamically unstable (G1, P1, E1). These instabilities are caused by aerodynamic forces on the hanging load and usually produce coupled oscillations involving yaw and lateral pendulum motions. Gabel and Wilson show experimentally that most hanging loads are aerodynamically stable over a wide speed range with a proper choice of cable configurations.

Before a load is moved, one should make sure that no aerodynamic instabilities exist up to the desired cruise speed. Some instabilities could probably be actively controlled if their nature were known in advance. However, it seems easier to avoid them in the speed range of interest.

Further work is required into the nature of these aerodynamic instabilities. Then, autopilot logic to eliminate these instabilities could be developed, and, with adequate redundancy in the control system, it would then be possible to carry hanging loads at even higher speeds without retracting the cables.

REFERENCES

B1 A. E. Bryson, Jr. and Y. C. Ho, Applied Optimal Control, Xerox Publishing Company, Lexington, Massachusetts, 1969

B2 A. E. Bryson, Jr. and W. E. Hall, Jr., "Optimal Control and Filter Synthesis by Eigenvector Decomposition," Stanford University, Department of Aeronautics and Astronautics, Report No. 436, Nov. 1971

D1 T. A. Dukes, "Maneuvering Heavy Sling Loads near Hover," presented at the 28th National Forum of the American Helicopter Society, Washington, D. C., Preprint No. 630, May 1972

E1 B. Etkin and J. C. Mackworth, "Aerodynamic Instability of Non-Lifting Bodies Towed Beneath an Aircraft," University of Toronto, Institute of Aerophysics, Technical Note No. 65, Jan. 1963

G1 R. Gabel and G. J. Wilson, "Test Approaches to External Sling Load Instabilities," Journal of the American Helicopter Society, Vol. 15, No. 3, July 1968, pp. 44-55

G2 A. Gessow and G. C. Meyers, Jr., Aerodynamics of the Helicopter, The McMillan Company, New York, 1952

H1 W. E. Hall, Jr., "Computational Methods for the Synthesis of Rotary Wing VTOL Aircraft Control Systems," Ph.D. Dissertation, Stanford University, August 1971

H2 W. E. Hall, Jr. and A. E. Bryson, Jr., "The Inclusion of Rotor Dynamics in Controller Design for Helicopters," Journal of Aircraft, Vol. 10, No. 4, April 1973, pp. 200-206

H3 W. E. Hall, Jr. and A. E. Bryson, Jr., "Synthesis of Hover Autopilots for Rotary-Wing VTOL Aircraft," Stanford University, Department of Aeronautics and Astronautics, Report No. 446, June 1972

K1 W. P. Keane and R. J. Milelli, "IFR Hover for Heavy Lift Helicopters with Slung Load," presented at the 27th Annual National V/STOL Forum of the American Helicopter Society, Washington, D. C., Preprint No. 540, May 1971

L1 L. R. Lucassen and F. J. Sterk, "Dynamic Stability Analysis of a Hovering Helicopter with a Slung Load," Journal of American Helicopter Society, Vol. 10, No. 2, April 1965, pp. 6-12

N1 A. A. Nikolsky, Helicopter Design, John Wiley and Sons, New York, 1951

P1 C. Poli and D. Cromack, "Dynamics of Slung Bodies Using a Single Point Suspension System," Journal of Aircraft, Vol. 10, No. 2, February 1973, pp. 80-86

S1 L. S. Szustak and D. S. Jenney, "Control of Large Crane Helicopters," Journal of the American Helicopter Society, Vol. 16, No. 3, July 1971, pp. 11-22

W1 J. Wolkovitch and D. E. Johnston et al., "Automatic Control Considerations for Helicopters and VTOL Aircraft With and Without Sling Loads," TR 138-1, Systems Technology Inc., Hawthorne, Calif., Nov. 1965, 155 pp.

W2 J. Wolkovitch, R. A. Peters and D. E. Johnston, "Lateral Control of Hovering Vehicles With and Without Sling Loads," TR 145-1, Systems Technology, Inc., Hawthorne, Calif., May 1966, 123 pp.

Appendix A

EIGENVALUES AND EIGENVECTORS OF THE OPEN-LOOP AND CLOSED-LOOP SYSTEMS

A.1 Open-Loop Systems

Eigenvalues and eigenvectors of the open-loop coupled and decoupled systems are given in Table A-1 in units of m , sec and radians .

Table A-1

OPEN-LOOP EIGENVALUES AND EIGENVECTORS

(a) Longitudinal System

Eigenvalue	Eigenvector			
sec^{-1}	θ_v	x_v	x_ℓ	V_{w_x}
$-.11 \pm 1.7j$	$.028 \mp .11j$	$-.040 \mp .59j$	$.025 \pm .16j$	0.0
$.095 \pm .26j$	$.0060 \mp .0044j$	$.87 \pm .11j$	1.0	0.0
-.40	-.11	.75	.55	0.0
0.0	0.0	-.71	-.71	0.0
-.20	.0028	-.72	-.66	.13

(b) Lateral System

Eigenvalue	Eigenvector			
sec^{-1}	ϕ_v	y_v	y_ℓ	V_{w_y}
$-.67 \pm 2.8j$	$-.095 \pm .17j$	$-.078 \mp .33j$	$.013 \pm .033j$	0.0
$.096 \pm .27j$	$-.0065 \pm .0044j$	$+.86 \pm .11j$	1.0	0.0
-.46	.014	.75	.51	0.0
0.0	0.0	-.71	-.71	0.0
-.20	-.0028	-.71	-.66	.14

[Units m , sec ; angles in rad]

Table A-1 (Cont'd)

(c) Coupled Longitudinal-Lateral System

Eigenvalue	Eigenvector							
sec^{-1}	θ_v	x_v	x_ℓ	V_{w_x}	ϕ_v	y_v	y_ℓ	V_{w_y}
$-.11 \pm 1.7j$	$-.026 \mp .11j$	$-.039 \mp .60j$	$+.026 \pm .16j$	0.0	$-.026 \mp .0052j$	$.16 \mp .011j$	$-.042 \pm .0074j$	0.0
$.076 \pm .26j$	$.0062 \mp .0035j$	$.86 \pm .088j$	1.0	0.0	$-.0043 \mp .0053j$	$.061 \pm .83j$	$.17 \pm .95j$	0.0
$-.68 \pm 2.9j$	$.026 \pm .0086j$	$.023 \mp .026j$	$-.0028 \pm .0023j$	0.0	$-.099 \pm .17j$	$-.075 \mp .32j$	$.012 \pm .031j$	0.0
$.11 \pm .28j$	$.0059 \pm .0046j$	$.045 \pm .75j$	$.19 \pm .84j$	0.0	$-.0067 \pm .0054j$	$.86 \pm .14j$	1.0	0.0
$-.42 \pm .10j$	$-.0093 \mp .011j$	$.22 \pm .87j$	$.071 \pm .64j$	0.0	$.015 \mp .0070j$	1.0	$.72 \pm .10j$	0.0
0.0	0.0	-.68	-.68	0.0	0.0	.21	.21	0.0
0.0	0.0	-.35	-.35	0.0	0.0	-.61	-.61	0.0
-.2	.0028	-.71	-.65	.14	-.00033	-.087	-.080	0.0
-.2	-.00028	.075	.069	0.0	-.0028	-.71	-.65	.15

[Units m , sec ; angles in rad]

A.2 Closed-Loop Systems

Table A-2 shows the eigenvalues and the corresponding eigenvectors of the decoupled and coupled longitudinal-lateral systems.

Table A-2

CLOSED-LOOP EIGENVALUES AND EIGENVECTORS

(a) Longitudinal System

Eigenvalue	Eigenvector			
sec^{-1}	θ_v	x_v	x_ℓ	V_{w_x}
$-.99 \pm 1.8j$	$.11 \mp .063j$	$-.24 \mp .43j$	$.064 \pm .020j$	0.0
$-.84 \pm .78j$	$.066 \mp .028j$	$-.64 \mp .60j$	$.13 \mp .26j$	0.0
$-.58 \pm 1.0j$	$.058 \mp .040j$	$-.42 \mp .74j$	$.34 \mp .076j$	0.0
$-.2$	.00026	-.0043	.0013	1.0

(b) Lateral System

Eigenvalue	Eigenvector			
sec^{-1}	Φ_v	y_v	y_ℓ	V_{w_y}
$-2.2 \pm 3.5j$	$-.20 \pm .097j$	$-.13 \mp .20j$	$.0074 \pm .0087j$	0.0
$-.82 \pm .74j$	$-.063 \pm .032j$	$-.67 \pm .61j$	$.12 \mp .29j$	0.0
$-.53 \pm 1.0j$	$-.050 \pm .043j$	$-.40 \mp .77j$	$.39 \mp .048j$	0.0
$-.2$	-.00026	-.0043	.0013	1.0

[Units m , sec ; angles in rad]

Table A-2 (Cont'd)

(c) Coupled Longitudinal-Lateral System

Eigenvalue	Eigenvector							
sec^{-1}	θ_v	x_v	x_ℓ	V_{w_x}	ϕ_v	y_v	y_ℓ	V_{w_y}
$-.93 \pm 1.9j$	$.11 \mp .070j$	$-.21 \mp .42j$	$.055 \pm .30j$	0.0	$.030 \mp .040j$	$.086 \pm .16j$	$-.024 \mp .0099j$	0.0
$-2.3 \pm 3.5j$	$.0088 \pm .032j$	$.028 \mp .046j$	$-.00046 \pm .0011j$	0.0	$-.21 \pm .092j$	$-.13 \mp .20j$	$.0069 \pm .0080j$	0.0
$-.92 \pm .62j$	$.067 \mp .021j$	$-.75 \mp .51j$	$-.00083 \mp .28j$	0.0	$-.011 \mp .057j$	$.50 \mp .50j$	$.22 \pm .043j$	0.0
$-.72 \pm .79j$	$.032 \pm .054j$	$.59 \mp .63j$	$.30 \pm .17j$	0.0	$-.059 \pm .035j$	$-.63 \mp .69j$	$.21 \mp .31j$	0.0
$-.58 \pm 1.1j$	$.057 \mp .044j$	$-.38 \mp .72j$	$.31 \mp .019j$	0.0	$.039 \pm .044j$	$-.62 \pm .30j$	$-.012 \mp .27j$	0.0
$-.50 \pm .98j$	$-.037 \mp .039j$	$-.61 \pm .42j$	$-.096 \mp .36j$	0.0	$-.049 \pm .040j$	$-.41 \mp .81j$	$.45 \mp .062j$	0.0
-.2	.00028	-.0076	-.0018	1.0	-.00035	-.0069	-.0064	0.0
-.2	-.00048	.0072	.0066	0.0	-.00028	-.0074	-.0016	1.0

[Units m , sec ; angles in rad]

Appendix B

TRANSFER FUNCTIONS OF COMPENSATORS FOR PRECISION HOVER IN THE PRESENCE OF CORRELATED WIND

B.1 Introduction

As indicated in Chapter 3, a filter-controller can be considered to be a multi-input multi-output compensator. A possible implementation is shown in figure B.1. In general this compensator has as many poles as the order of the system (except with pole-zero cancellations) and each term has at least one less zero than the number of poles. The compensator transfer function matrix is

$$\Delta_c = C\{sI - (F+GC-KH)\}^{-1}K \qquad (B.1)$$

and is the transfer function between the measurements and control.

B.2 Compensators for Longitudinal and Lateral Systems

The transfer function matrix of the compensator for both the longitudinal and the lateral systems is a 1X3 matrix. Each term has seven poles and six zeroes. The poles of the three terms are, of course, the same. The pole-zero location of the terms in the longitudinal system are shown in figures B.2 to B.4 and of the lateral system are shown in figures B.5 to B.7. All elements in the transfer function matrices of the two systems have poles in the right half plane. Some elements have a pair of zeroes also in the right half plane. Such compensators are said to have non-minimum phase.

It is clear that the closed-loop system has fourteen poles, seven of them can be identified with the controller and the remaining seven with the filter. All these fourteen poles lie in the left half plane and the closed-loop system is stable.

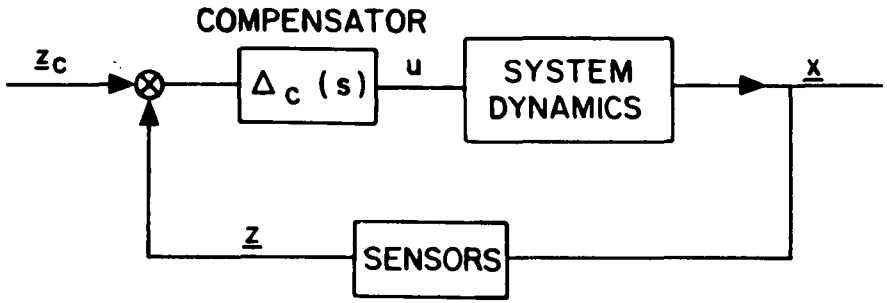

FIG. B.1 Precision Hover Autopilot as a Multi-Input Multi-Output Compensator

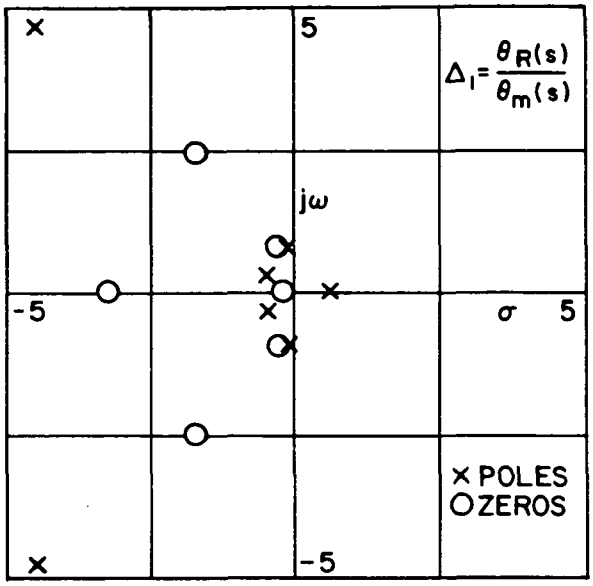

FIG. B.2 Compensator Transfer Function Δ_1 for Longitudinal System

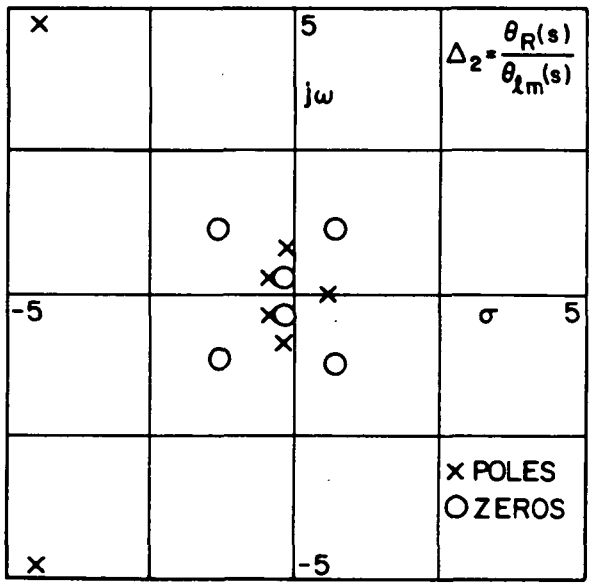

FIG. B.3 Compensator Transfer Function Δ_2 for Longitudinal System

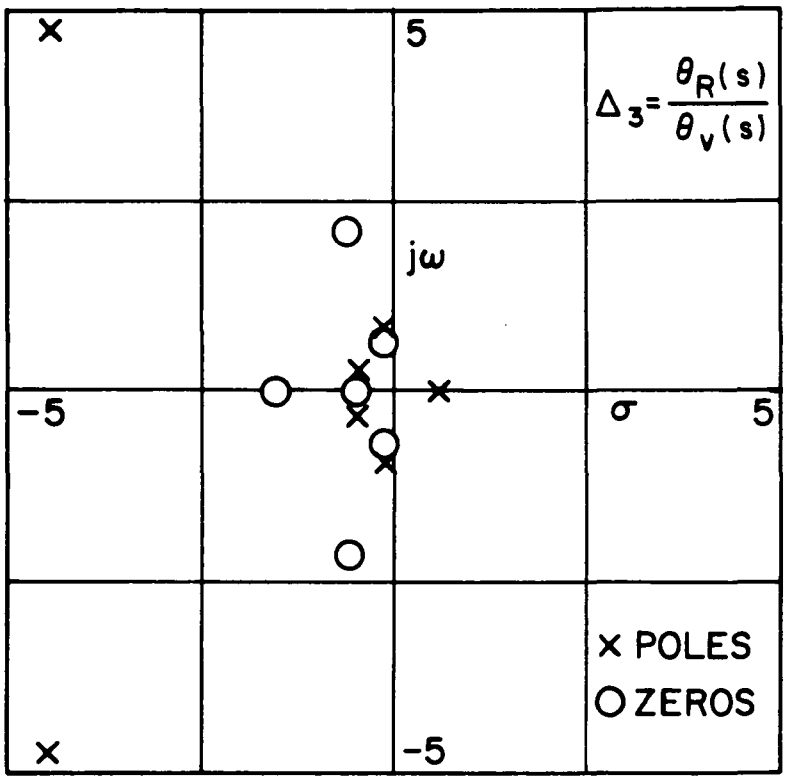

FIG. B.4 Compensator Transfer Function Δ_3 for Longitudinal System

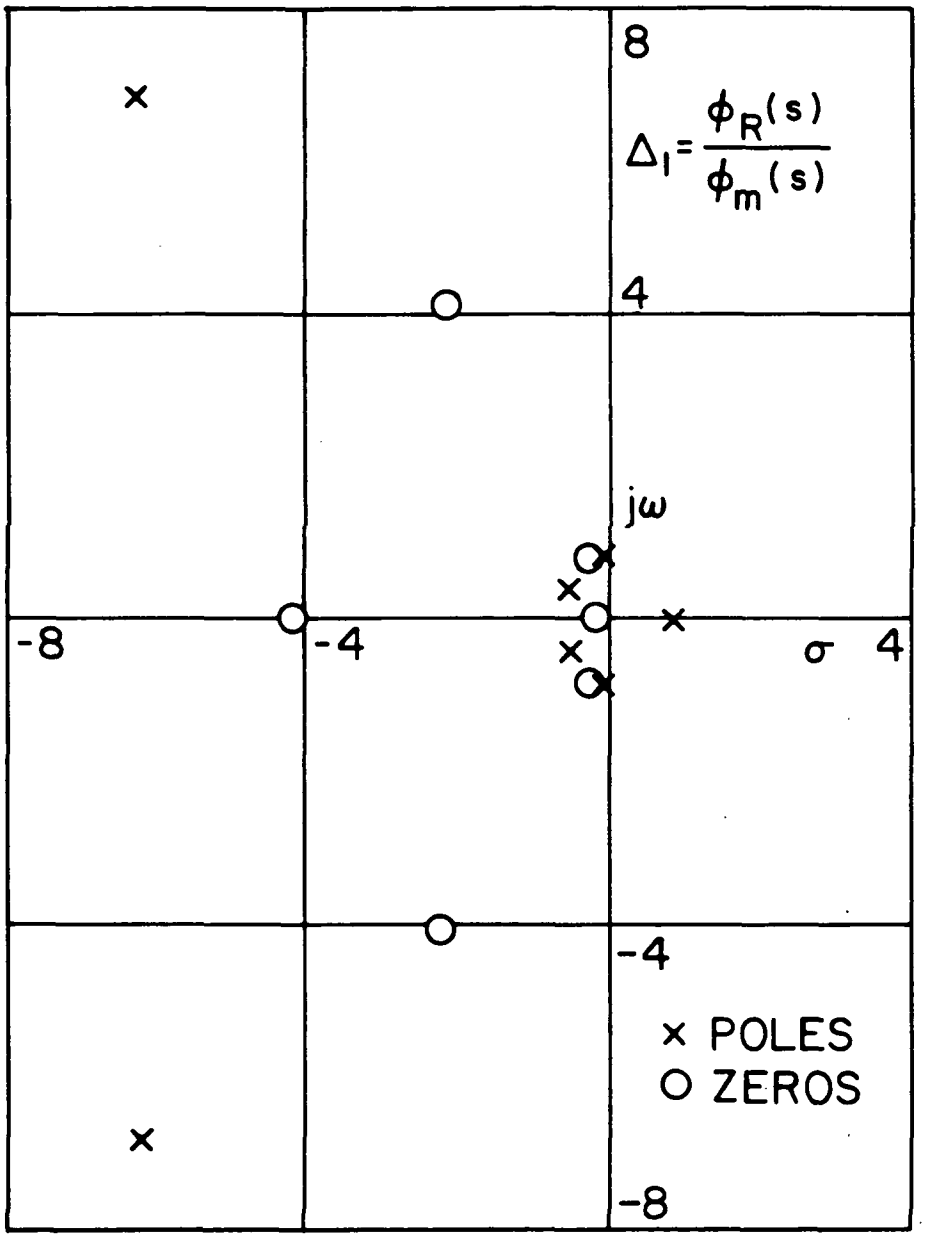

FIG. B.5 Compensator Transfer Function Δ_1 for Lateral System

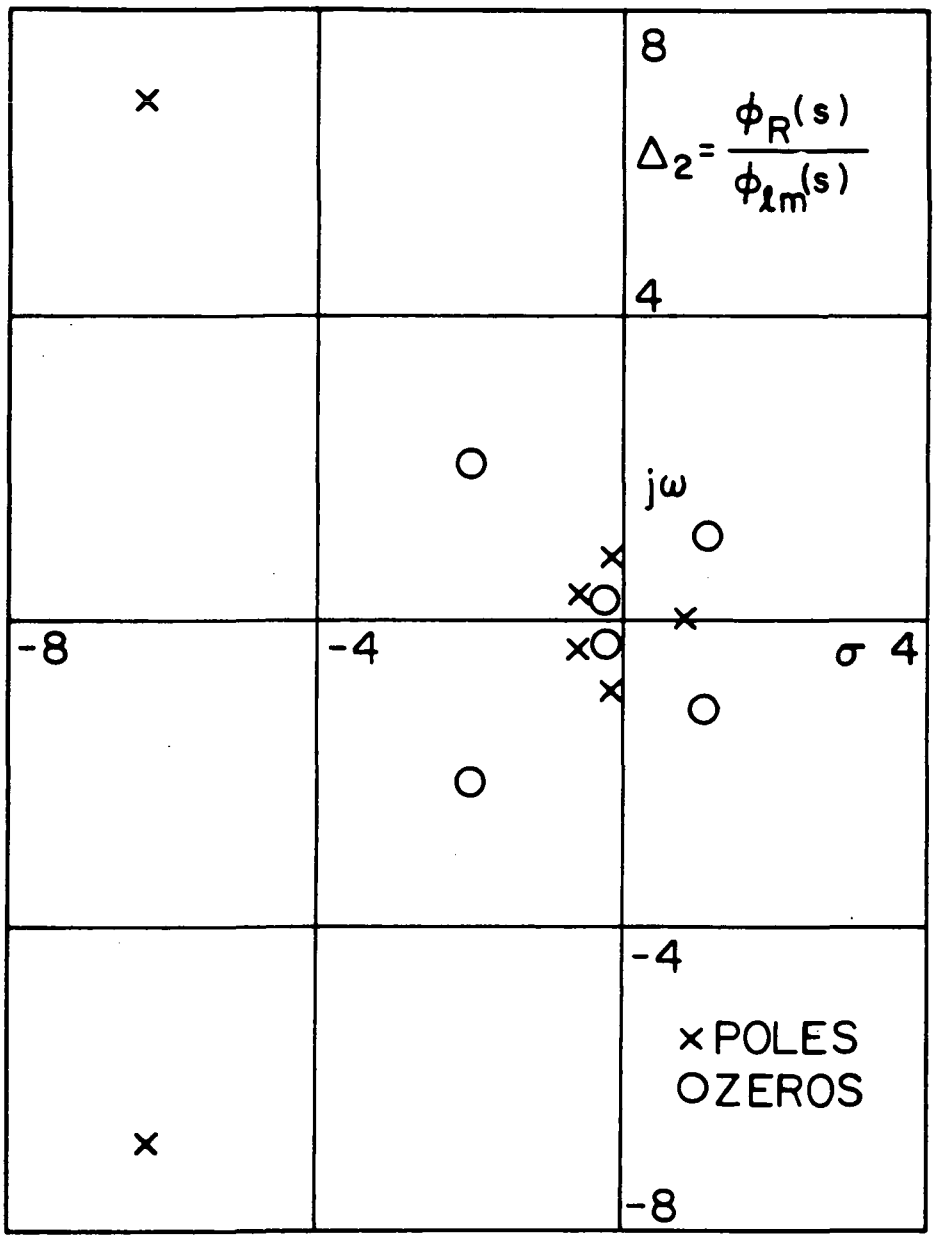

FIG. B.6 Compensator Transfer Function Δ_2 for Lateral System

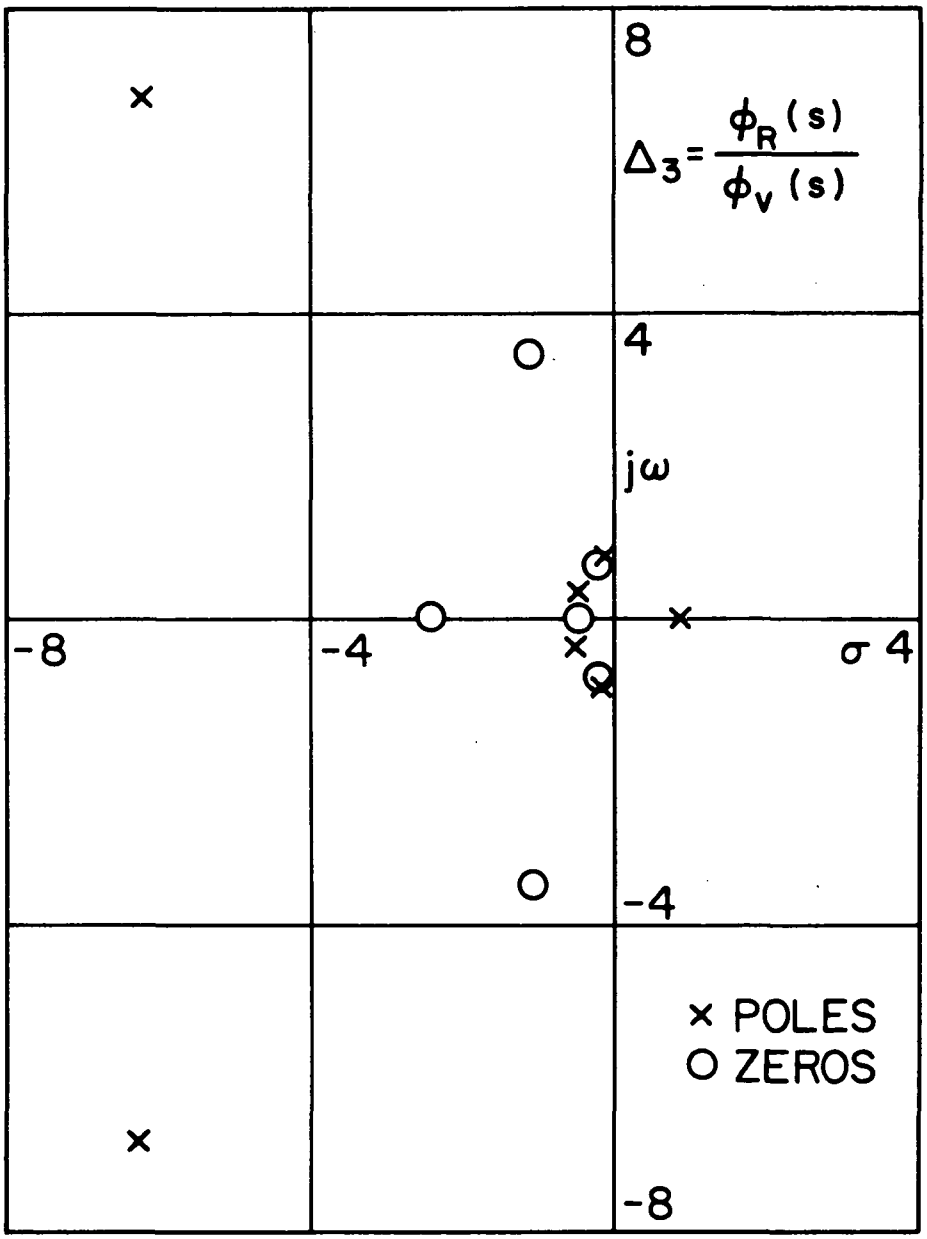

FIG. B.7 Compensator Transfer Function Δ_3 for Lateral System

These compensators cannot be tested directly since they are "unstable". One way to test them is to close the loop by using a simulation of the system. The response of the closed-loop system to initial errors and random disturbances can then be checked.

Appendix C

A TECHNIQUE FOR FINDING FEEDBACK GAINS FOR CORRELATED DISTURBANCES

C.1 Introduction

Consider a system

$$\dot{\underline{x}} = F\underline{x} + G\underline{u} + \Gamma\underline{w} \quad * \tag{C.1}$$

in which $\underline{u}$ is an m control vector and $\underline{w}$ is a p disturbance vector obeying the equation

$$\dot{\underline{w}} = E\underline{w} + \underline{\eta} \tag{C.2}$$

$\underline{\eta}$ is white noise. If we choose

$$\underline{u} = C\underline{x} + C_w\underline{w} \tag{C.3}$$

in the steady state we have

$$F_c X_{xx} + X_{xx} F_c^T + \Gamma_c X_{xw}^T + X_{xw}\Gamma_c^T = 0 \tag{C.4}$$

$$F_c X_{xw} + X_{xw} E^T + \Gamma_c X_{ww} = 0 \tag{C.5}$$

where

---

*With noisy measurements and optimal filter (See (C.6) for definition)

$$X_{xx} = X_{\hat{x}\hat{x}} + X_{\tilde{x}\tilde{x}}$$

where $\hat{\underline{x}}$ is the estimate of $\underline{x}$ and $\tilde{\underline{x}}$ is the estimation error. $X_{\tilde{x}\tilde{x}}$ depends on state and measurement noise. Choice of gains C_w only changes $X_{\hat{x}\hat{x}}$. The equation governing $\hat{\underline{x}}$ is

$$\dot{\hat{\underline{x}}} = F\hat{\underline{x}} + G\underline{u} + K\underline{\nu} - KH\hat{\underline{x}}$$

$$X_{ab} = E(ab^T)$$

$$F_c = F + GC \tag{C.6}$$

$$\Gamma_c = \Gamma + GC_w$$

We choose gains C first to obtain the desired closed-loop dynamics. The gains C_w can subsequently be chosen to reduce the effect of wind as much as possible, i.e., if $T\underline{x}$ are q independent linear combinations of the states we are interested in, C_w could be chosen to minimize

$$L = Tr\ \ E\{(T\underline{x})^T DT\underline{x}\}\ s.s. \quad = Tr\{T^T DTX_{xx}\} \tag{C.7}$$

where D is $q \times q$ positive definite weighting matrix. Thus the Hamiltonian is

$$H = L + Tr\left[\{F_c X_{xx} + X_{xx}F_c^T + \Gamma_c X_{xw}^T + X_{xw}\Gamma_c^T\}\Lambda + \{F_c X_{xw} + X_{xw}E^T + \Gamma_c X_{ww}\}\lambda\right] \tag{C.8}$$

Here Λ and λ are Lagrange multiplier matrices. The required optimization equations are

(α) (C.4) and (C.5)

(β) $$\frac{\partial H}{\partial X_{xx}} = 0 \Rightarrow F_c^T\Lambda + \Lambda F_c + T^T DT = 0 \tag{C.9}$$

$$\frac{\partial H}{\partial X_{xw}} = 0 \Rightarrow 2\Lambda\Gamma_c + F_c^T\lambda + \lambda E = 0 \tag{C.10}$$

(γ) $$\frac{\partial H}{\partial C_w} = 0 \Rightarrow 2G^T\Lambda X_{xw} + G^T\lambda^T X_{ww} = 0 \tag{C.11}$$

Comments on solving the optimization equations:

1. Equation (C.9) can be solved for Λ.
2. Equation (C.4) can be solved in the end since no other equation involves X_{xx}.

3. (C.5), (C.10) and (C.11) are $(2n+m)p$ equations in $(2n+p)m$ unknowns X_{xw}, λ and C_w.

4. These equations assure a solution for well posed problems (i.e., negative definite F_c and negative semidefinite E, positive definite X_{ww} and finite, nonzero G). However, the solution may not be unique. Any nonuniqueness can be resolved by minimizing $\underline{u}^T B \underline{u}$.

5. If the space spanned by vectors in G contains the space spanned by vectors in Γ, then one solution is to choose C_w such that $\Gamma + GC_w$ is zero, in which case $L = 0$.

C.2 Random Bias Disturbance

For bias disturbances the matrix E is zero and $\eta = 0$. Then since F_c is negative definite and hence invertible, equations (C.5) and (C.10) can be solved directly.

$$X_{xw} = -F_c^{-1}\Gamma_c X_{ww}$$

$$\lambda = -2F_c^{-1}\Lambda\Gamma_c^T \qquad \text{(C.12)}$$

Substituting (C.12) and (C.9) in (C.11) gives

$$MC_w + N = 0 \qquad \text{(C.13)}$$

where

$$M = G^T F_c^{-T} T^T D T F_c^{-1} G$$

$$N = G^T F_c^{-T} T^T D T F_c^{-1} \Gamma \qquad \text{(C.14)}$$

The solution is unique if M has rank m, i.e., if

$$\text{rank}(M) = \text{rank}(G^T F_c^{-T} T^T) = m \qquad \text{(C.15)}$$

The rank of M cannot exceed m, which is the rank of G. If there are exactly m disturbances and M has rank m

$$C_w = -(TF_c^{-1}G)^{-1} TF_c^{-1}\Gamma \qquad \text{(C.16)}$$

C.3 Independent Disturbances

The design procedure is simplified when the p disturbances are independent, i.e., E and X_{ww} are diagonal (this generalizes to the case where E and X_{ww} are block diagonal with the same block sizes). Then the gains on each disturbance can be chosen independently. To find gains on any particular disturbance we proceed as follows.

In our general formulas, we consider p equal to one and E and X_{ww} scalars. (C.5) and (C.10) become

$$(F_c+EI)X_{xw} + \Gamma_c X_{ww} = 0$$

$$(F_c+EI)^T\lambda + 2\Lambda\Gamma_c = 0$$

or

$$X_{xw} = -(F_c+EI)^{-1}\Gamma_c X_{ww}$$

$$\lambda = -2(F_c+EI)^{-T}\Lambda\Gamma_c \qquad (C.17)$$

Substituting in (C.11) we have

$$MC_w + N = 0 \qquad (C.18)$$

where

$$M = G^T F_{ce}^T (T^T DT - 2E\Lambda)F_{ce}G$$

$$N = G^T F_{ce}^T (T^T DT - 2E\Lambda)F_{ce}\Gamma$$

and $F_{ce} = (F_c + EI)^{-1}$ (C.19)

Nonuniqueness can be resolved as in section (C.1).

Appendix D

VELOCITY HOLD AUTOPILOTS FOR LOW SPEED

D.1 Design

A velocity-hold autopilot maintains the vehicle speed near a desired value. With no constraint on time, we are not interested in errors in horizontal position. Thus the state equations of Chapter II can be rewritten in terms of the state variable vectors, $(\theta_v, \dot{\theta}_v, \dot{x}_v, \theta_\ell, \dot{\theta}_\ell)^T$ and $(\phi_v, \dot{\phi}_v, \dot{y}_v, \dot{\phi}_\ell, \phi_\ell)^T$. Now in addition to the measurements of four angles $\theta_\ell, \theta_v, \phi_\ell$ and ϕ_v we need measurements of longitudinal and lateral velocities. Noise in measurement of velocity is assumed to be white with power spectral density $.005\ m^2 sec^{-1}$. The state definition matrices and the measurement distribution matrices are shown in Table D-1. We estimate that in the speed range of interest the drag coefficient terms on the vehicle and the load do not change substantially. Small changes will not deteriorate the performance very much as has been shown for the precision hover autopilot.

The lateral velocity is usually maintained at zero while the longitudinal velocity is held at the desired cruise speed.

Both longitudinal and lateral systems are augmented with a state variable corresponding to wind velocity. The control systems are designed using quadratic synthesis. The feedback controller gains are presented in Table D-2. Also shown are the open-loop and closed-loop eigenvalues. All modes of the closed-loop system have adequate damping.

Filters are designed based on the measurements given above in the presence of wind with RMS intensity $7.0\ m\ sec^{-1}$ and correlation time 5 sec. Filter gains and characteristic roots of the estimate error equation are given in Table D-2.

Table D-1

State Definition Matrices for Velocity Hold Autopilots

LONGITUDINAL SYSTEM

F:					$\underline{\dot{x}}$	G	Γ	H:		
0.0	1.0	0.0	0.0	0.0	θ_v	0.0	0.0	0.0	1.0	0.0
-2.09	-.415	.0111	2.09	0.0	$\dot{\theta}_v$	8.38	-.0111	0.0	0.0	0.0
-13.1	1.43	-.0198	3.28	0.0	$\dot{x}_v$	-13.1	.0198	0.0	0.0	1.0
0.0	0.0	0.0	0.0	1.0	θ_ℓ	0.0	0.0	1.0	0.0	0.0
.812	-.0405	.0000288	-.812	-.0026	$\dot{\theta}_\ell$	.0265	-.0000288	0.0	0.0	0.0

$\underline{x}^T = [\theta_v \quad \dot{\theta}_v \quad x_v \quad \theta_\ell \quad \dot{\theta}_\ell]$ $\quad [u_1 \approx \theta_R]$ $\quad [V_{w_x}]$ $\quad \underline{z} = [\theta_\ell \ , \ \theta_v \ , \ \dot{x}_v]^T$

LATERAL SYSTEM

F:					$\underline{\dot{x}}$	G	Γ	H:		
0.0	1.0	0.0	0.0	0.0	ϕ_v	0.0	0.0	0.0	1.0	0.0
-7.70	-1.58	-.0407	7.7	0.0	$\dot{\phi}_v$	30.8	.0407	0.0	0.0	0.0
13.1	-1.43	-.0198	-3.28	0.0	$\dot{x}_v$	13.1	.0198	0.0	0.0	1.0
0.0	0.0	0.0	0.0	1.0	ϕ_ℓ	0.0	0.0	1.0	0.0	0.0
1.21	.0468	.00219	-1.21	-.0026	$\dot{\phi}_\ell$	-1.655	-.00219	0.0	0.0	0.0

$x^T = [\phi_v \quad \dot{\phi}_v \quad \dot{y}_v \quad \phi_\ell \quad \dot{\phi}_\ell]$ $\quad [u_2 \approx \phi_R]$ $\quad [V_{w_y}]$ $\quad \underline{z} = [\phi_\ell \ , \ \phi_v \ , \ \dot{y}_v]^T$

(Units in m , sec ; angles in rad)

Table D-2

Controllers and Filters for Velocity Hold Autopilots

$$J_{long.} = \{\ 100\ \theta_v^2 + \dot{x}_v^2 + 200\ \theta_\ell^2 + 100\ u_1^2\ \}_{s.s.}$$

$$J_{lat.} = \{\ 100\ \phi_v^2 + \dot{y}_v^2 + 200\ \phi_\ell^2 + 100\ u_2^2\ \}_{s.s.}$$

Feedback Gains

C_{θ_v}	$C_{\dot{\theta}_v}$	$C_{\dot{x}_v}$	C_{θ_ℓ}	$C_{\dot{\theta}_\ell}$	C_{w_x}	C_{ϕ_v}	$C_{\dot{\phi}_v}$	$C_{\dot{y}_v}$	C_{ϕ_ℓ}	$C_{\dot{\phi}_\ell}$	C_{w_y}
-1.70	-.431	.0981	-.714	-.901	.00174	-1.39	-.242	-.0981	-.912	-.824	-.00172

$$K_{long.}^T = \begin{bmatrix} .0192 & -.0166 & -.872 & .260 & .0392 & 29.0 \\ 3.19 & 5.68 & -19.6 & .0770 & .541 & -886 \\ -.0600 & -.0914 & .908 & -.0107 & -.0315 & 20.4 \end{bmatrix}$$

$$K_{lat.}^T = \begin{bmatrix} -.0190 & -.0802 & .793 & .263 & .0391 & -45.2 \\ 4.11 & 8.85 & 16.1 & -.076 & .145 & 985 \\ .0493 & .0580 & .834 & .0097 & .0302 & 11.8 \end{bmatrix}$$

Eigenvalues (sec^{-1})

Longitudinal System	Open-Loop	$-.11 \pm 1.7j$	$.098 \pm .26j$	-.41	-.20
	Closed-Loop	$-1.5 \pm 2.3j$	$-.40 \pm .64j$	-1.6	-.20
	Estimate Error	$-.95 \pm 2.3j$	$-.25 \pm .79j$	-1.9	-.70
Lateral System	Open-Loop	$-.67 \pm 2.8j$	$.098 \pm .27j$	-.46	-.20
	Closed-Loop	$-.34 \pm 4.4j$	$-.38 \pm .63j$	-1.45	-.20
	Estimate Error	$-1.5 \pm 3.7j$	$-.24 \pm .77j$	-2.9	-.67

(Units in m , sec ; angles in rad)

D.2 Performance

The performance of the system is computed with perfect state information (ideal case) and with noisy measurements and filter. Table D-3 shows the results. The performance is satisfactory. Major improvements in RMS response can be affected only by improving the measurements.

Table D-3

RMS Errors for the Longitudinal and Lateral Systems

	θ_v	$\dot{\theta}_v$	$\dot{x}_v$	θ_ℓ	$\dot{\theta}_\ell$	u_1
Perfect State Information	.00173	.00148	.0171	.00197	.00085	.00931
Noisy Measurement and Filter	.0143	.0379	.136	.0095	.0094	.0189

	Φ_v	$\dot{\Phi}_v$	$\dot{y}_v$	Φ_ℓ	$\dot{\Phi}_\ell$	u_2
Perfect State Information	.00173	.00217	.0166	.00194	.00085	.00928
Noisy Measurement and Filter	.0140	.0566	.119	.0081	.0093	.0146

(Units in m , sec ; angles in rad)